

Mechanically Interlocked Polymers in Dilute Solution under Shear and Extensional Flows: A Brownian Dynamics Study

Ali Seyedi, Alex Albaugh*

*Department of Chemical Engineering and Materials Science,
Wayne State University, 5050 Anthony Wayne Drive, Detroit, Michigan 48202, USA*

Mechanically interlocked polymers (MIPs) are a novel class of polymer structures in which the components are connected by mechanical bonds instead of covalent bonds. We measure the single-molecule rheological properties of polyrotaxanes, daisy chains, and polycatenanes under steady shear and steady uniaxial extension using coarse-grained Brownian dynamics simulations with hydrodynamic interactions. We obtain key rheological features, including tumbling dynamics, molecular extension, stress, and viscosity. By systematically varying structural features, we demonstrate how MIP topology governs flow response. Compared to linear polymers, all three MIP architectures exhibit enhanced tumbling in shear flow and lower normal stress differences in extensional flow. While polyrotaxanes show higher shear and extensional viscosities, polycatenanes and daisy chains have lower viscosities. In extensional flow, polyrotaxanes and polycatenanes extend earlier than linear polymers. We find that mechanical bonds suppress shear thinning and alter the coil-stretch transition observed in linear polymers. These effects arise from the mechanically bonded rings in MIPs, which expand the polymer profile in gradient direction and increase backbone stiffness due to ring-backbone repulsions. This study provides key insights into MIP flow properties, providing the foundation for their systematic development in engineering applications.

I. INTRODUCTION

Mechanically interlocked polymers (MIPs) are an emerging class of polymer architectures distinguished by components linked through mechanical entanglements rather than covalent bonds. These unique structural features impart MIPs with increased conformational freedom, setting them apart from typical polymers [1] and leading to unique properties[2, 3] such as shape memory, ductile glassy states, large strain-at-break, scratch resistance, and stimuli-responsive mechanical properties. Theoretical and computational studies have further indicated that they have large loss modulus, low activation energy for viscous flow, superior energy-damping, and excellent toughness[1, 4, 5].

The schematic representation in Fig. 1 shows different classes of MIPs in comparison with a linear polymer (Fig. 1a). Polyrotaxanes (Fig. 1b) consist of multiple ring-shaped molecules threaded onto a linear backbone, held in place by bulky end caps called stoppers[6, 7]. Daisy chains (Fig. 1c) are made from covalently-bonded rings and linear sections interlocked in series[8, 9]. Polycatenanes (Fig. 1d) are polymers made of interlocked rings, like a chain[5, 10–12]. Although mechanically interlinking molecules (catenation) is a synthetic challenge [13, 14], recent advances have enabled the production of MIPs with moderate molecular weights. The largest polyrotaxane synthesized to date has weight-average molecular weight $M_w = 119,000$ g/mol with 86 threaded rings [15] while the largest daisy chain polymer has 11 repeat units and number-average molecular weight $M_n \approx 25,000$ g/mol [16]. The longest linear and branched polycatenanes ever built have 26 and 130 rings in their structures with $M_n \approx 40,000$ g/mol and $M_n \approx 200,000$ g/mol, respectively [5]. Nano-scale polycatenanes comprising up to 22 interlocked rings have been

synthesized through the self-assembly of supramolecular toroidal building blocks [17].

Despite advances in synthesis, the relationship between mechanical bonds and flow properties is largely unexplored. Such properties need to be measured to develop MIPs for practical applications. Computational techniques present an effective method to link the molecular structure, dynamics, and macroscopic behavior of polymers[18–22]. In the realm of MIPs, computational research has quantified the structural and dynamic properties of doubly interlocked rings (2-catenanes) in equilibrium conditions [23, 24], in shear [25], and in glassy states [26]. Simulation studies have explored the equilibrium behavior of longer polycatenanes (up to 300 rings), isolated [27–32] and in a melt state [33–35], uncovering characteristics that blend features of ring and linear polymers. In addition, computational investigations have probed the structure and dynamics of catenanes under confinement [36] and during pore translocation [37, 38] and rotaxanes have been analyzed in equilibrium [39, 40]. These simulations have highlighted the unique behavior of MIPs compared to conventional polymers, demonstrating how structural features, such as ring size and the number of mechanical bonds, influence properties like chain stiffness, θ -temperature, and relaxation dynamics. Importantly, these studies show that MIPs exhibit emergent properties not observed in typical linear and cyclic polymer architectures, highlighting the crucial role of topology in governing their behavior.

Here we simulate MIPs with coarse-grained Brownian dynamics, an approach that has been effective at characterizing the rheology of many polymer morphologies, like linear, combs, bottlebrushes, and ring polymers[41–44]. We report rheological properties for polyrotaxanes, daisy chains, and polycatenanes in both steady shear and steady extensional flow, a critically uncharacterized do-

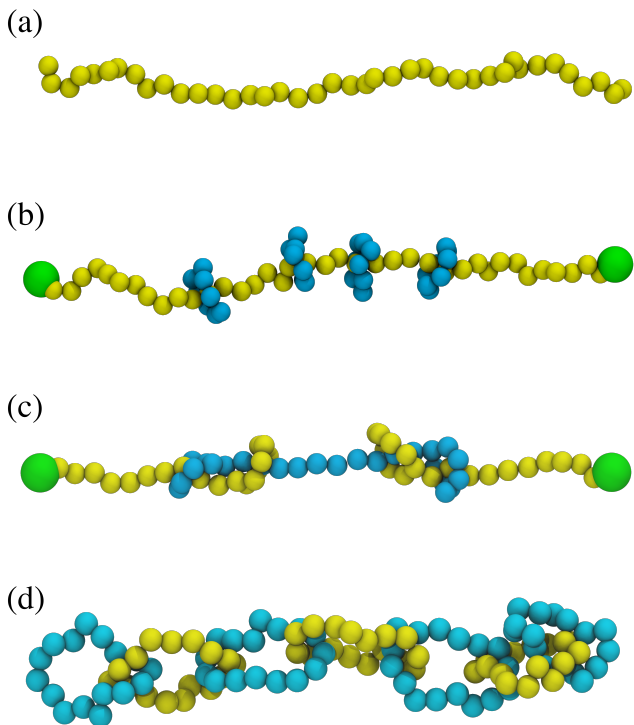


FIG. 1: Schematic representation of polymers: (a) linear polymer, (b) polyrotaxane, (c) daisy chain, and (d) polycatenane. Yellow and blue beads are equivalent, the colors are chosen to highlight the interlocked architecture. Green beads are large end caps to prevent dethreading in polyrotaxanes and daisy chains.

main for MIPs. Our results are a first step to understanding how MIPs will behave during processing as extensional flows are commonly encountered in blow molding, fiber spinning, film blowing, and foaming [45–47] and shear flows appear in injection molding and extrusion [48]. We show that all three MIP types show enhanced tumbling in shear flow and lower normal stress differences in extensional flow. Also, while polyrotaxanes show higher viscosity both in shear and extension, polycatenanes and daisy chains exhibit lower viscosities. In addition, polyrotaxanes and polycatenanes have an earlier onset of extension than linear polymers under extensional flow.

II. METHODS

We simulated single polymers in the dilute solution limit with a coarse-grained bead-based model. Polymers are composed of N beads that interact through bonded and non-bonded potentials. The pairwise non-bonded interaction potential is defined by the Weeks–Chandler–Anderson potential [49]

$$U_{\text{WCA}} = \sum_{\substack{i,j \\ j>i}} \begin{cases} 4\epsilon \left[\left(\frac{\sigma}{r_{ij}} \right)^{12} - \left(\frac{\sigma}{r_{ij}} \right)^6 \right] - U_c, & r_{ij} < r_c \\ 0, & r_{ij} \geq r_c \end{cases} \quad (1)$$

where $r_{ij} = |\mathbf{r}_j - \mathbf{r}_i|$ is the distance between particles i and j , r_c is the cutoff distance, $U_c = 4\epsilon \left[\left(\frac{\sigma}{r_c} \right)^{12} - \left(\frac{\sigma}{r_c} \right)^6 \right]$ is the Lennard-Jones energy at the cutoff distance, and σ and ϵ are the Lennard-Jones length and energy parameters, respectively. To prevent the rings from dethreading, the non-bonded interactions between capping beads and ring beads are scaled by a factor of 10^5 and 10^{10} in daisy chains and polyrotaxanes, respectively. Bonds between beads are modeled with finitely extensible nonlinear elastic (FENE) springs [22]:

$$U_{\text{FENE}} = - \sum_{i,j} \frac{1}{2} k_s r_{\max}^2 \log \left[1 - \left(\frac{r_{ij}}{r_{\max}} \right)^2 \right], \quad r_{ij} < r_{\max}, \quad (2)$$

where $k_s = 30\epsilon/\sigma^2$ is the spring strength and $r_{\max} = 1.5\sigma$ is the maximum bond extension. This model and parameterization has been used to model MIPs [33, 50]. The positions of beads evolve according to the following stochastic differential equation incorporating hydrodynamic interactions [51, 52]:

$$d\mathbf{r} = \left[\mathbf{v} + \frac{1}{k_B T} \mathbf{D} \cdot \mathbf{f} \right] dt + \sqrt{2} \mathbf{B} \cdot d\mathbf{w}, \quad (3)$$

where \mathbf{r} is a vector of particle positions with $3N$ elements, \mathbf{v} is the solvent flow velocity at the particle positions, \mathbf{f} is a vector of forces acting on the particles, \mathbf{D} is the diffusivity matrix, $\mathbf{B} = \sqrt{\mathbf{D}}$, and \mathbf{w} is a vector containing independent Wiener processes with zero mean and variance dt . In Eq. 3, the deterministic drift is calculated by the term within the square brackets, while the other term accounts for the Brownian motion of the particles due to random collisions with solvent molecules. The force vector is $\mathbf{f} = -\nabla U$, where $U = U_{\text{WCA}} + U_{\text{FENE}}$ is the total intramolecular potential. The matrix \mathbf{D} incorporates hydrodynamic interactions between the particles. Each 3×3 block of the matrix \mathbf{D} represents hydrodynamic interactions between particles i and j and is given by

$$\mathbf{D}_{ij} = \frac{k_B T}{\zeta} [(1 - \delta_{ij}) \mathbf{\Omega}_{ij} + \delta_{ij} \mathbf{I}], \quad i, j = 1, \dots, N, \quad (4)$$

where δ_{ij} is the Kronecker delta, \mathbf{I} is the 3×3 identity matrix, ζ is the friction coefficient, $a = \sigma/2$ is the hydrodynamic radius, and

$$\mathbf{\Omega}_{ij} = \begin{cases} \frac{3a}{4r_{ij}} \left[\left(1 + \frac{2a^2}{3r_{ij}^2} \right) \mathbf{I} + \left(1 - \frac{2a^2}{r_{ij}^2} \right) \frac{\mathbf{r}_{ij} \mathbf{r}_{ij}}{r_{ij}^2} \right], & r_{ij} \geq 2a, \\ \left(1 - \frac{9r_{ij}}{32a} \right) \mathbf{I} + \left(\frac{3r_{ij}}{32a} \right) \frac{\mathbf{r}_{ij} \mathbf{r}_{ij}}{r_{ij}^2}, & r_{ij} < 2a, \end{cases} \quad (5)$$

is the Rotne–Prager–Yamakawa tensor [53, 54]. To remove the overall translational motion of the molecule, the solvent velocity is centered around the center-of-mass of the polymer $\mathbf{r}_{\text{COM}} = [x_{\text{COM}}, y_{\text{COM}}, z_{\text{COM}}]^\top$ [55]. Thereby, the solvent velocity \mathbf{v}_i for bead i with spatial coordinate $\mathbf{r}_i = [x_i, y_i, z_i]^\top$ is zero at equilibrium; $[\dot{\gamma}(y_i - y_{\text{COM}}), 0, 0]^\top$ in shear flow, where $\dot{\gamma}$ is the shear rate; and $[\dot{\epsilon}(x_i - x_{\text{COM}}), -\dot{\epsilon}(y_i - y_{\text{COM}})/2, -\dot{\epsilon}(z_i - z_{\text{COM}})/2]^\top$ in uniaxial extensional flow, where $\dot{\epsilon}$ is the extension rate. Furthermore, the Weissenberg number (Wi) measures the flow strength and is defined as $\dot{\gamma}\tau_R$ for shear flow and $\dot{\epsilon}\tau_R$ for uniaxial extensional flow, where τ_R is the longest relaxation time of the polymer as calculated from $\tau_R = R_g^2/6D_{\text{COM}}$ where the center-of-mass diffusivity was calculated from the equilibrium conformations using the Kirkwood formalism [56]. Relaxation time results are summarized in tables A.1 to A.4. The variables are nondimensionalized using a as the unit of length, $k_B T$ as the unit of energy, and the diffusion time of a bead $\tau = \zeta a^2/k_B T$ as the unit of time. Eq. 3 is integrated numerically using a semi-implicit Euler scheme [57, 58] to allow the use of larger time steps compared to explicit methods. The diffusivity matrix \mathbf{D} and the Brownian term are treated explicitly and the remaining terms are treated implicitly.

The following set of nonlinear algebraic equations in \mathbf{r}^* are obtained using the semi-implicit algorithm:

$$\mathbf{r}^*(t^* + \Delta t^*) = \mathbf{r}^*(t^*) + \sqrt{2\Delta t^*} \mathbf{B}^*(t^*) \cdot \Delta \mathbf{w}^* + \left[\mathbf{v}^*(t^* + \Delta t^*) + \mathbf{D}^*(t^*) \cdot \mathbf{f}^*(t^* + \Delta t^*) \right] \Delta t^* \quad (6)$$

where Δt^* is the time step, $\Delta \mathbf{w}^*$ is a vector of normally-distributed random numbers with zero mean and unit variance, and the star represents non-dimensional quantities. \mathbf{B}^* is calculated at time t^* using Cholesky decomposition of \mathbf{D}^* .

Equation 6 is solved iteratively by a Jacobian-free Newton–Krylov method [59] through the NITSOL software package [60] without using a preconditioner. This approach has recently been used to simulate bottlebrush polymers [44]. We use OpenMP shared memory parallelism with 1-4 CPUs per simulation (depending on system size) to more efficiently calculate forces, perform the Cholesky decomposition of the \mathbf{D}^* matrix, and integrate the equation of motion. Initial configurations were generated with equilibrium bond lengths and energy minimization was carried out prior to production simulations. All properties were calculated by averaging over 10 to 20 trajectories of at least 100 relaxation times long ($10^6 - 10^8$ time steps) with time steps ranging from 10^{-2} to 10^{-4} depending on the strain rate. The fractional extension is defined as $\langle X_{bb} \rangle / L$ where X_{bb} is the difference between minimum and maximum coordinates in the x direction and L is the maximum contour length, calculated as $L = 3a(N_{\text{eff}} - 1)$. N_{eff} is effective number of beads which is determined differently depending on the polymer type. For linear polymers, $N_{\text{eff}} = N$ is the total number of beads. In the case of polyrotaxanes,

$N_{\text{eff}} = N_{bb}$ is the number of beads in the linear backbone. For polycatenanes, $N_{\text{eff}} = N/2$ is calculated as the total number of beads divided by 2. This adjustment accounts for the contour length of ring polymers, which is considered to be half the contour length of the corresponding linear polymer [61]. For daisy chains, L is calculated separately for the rings and the linear segments and then summed.

In dilute polymer solutions, the polymer contribution to the stress tensor ($\boldsymbol{\tau}^p$) is calculated using the following equation [62–64]

$$\frac{\boldsymbol{\tau}^p}{n_p k_B T} = -(N - 1) \mathbf{I} - \sum_{i=1}^{N-1} \sum_{j=i+1}^N \mathbf{f}_{ij}^* \mathbf{r}_{ij}^*$$

where n_p is the polymer number density, $\mathbf{r}_{ij}^* = \mathbf{r}_j^* - \mathbf{r}_i^*$ is the non-dimensionalized distance vector, and \mathbf{f}_{ij}^* is the non-dimensionalized force on bead i due to bead j . From this, we can obtain the shear stress τ_{xy} and the first normal stress difference, $N_1 = \tau_{xx}^p - \tau_{yy}^p$. The uniaxial extensional viscosity is $\eta_E = N_1/\dot{\epsilon}$, shear viscosity is $\eta = \tau_{xy}^p/\dot{\gamma}$, and the first normal stress coefficient is $\psi_1 = N_1/\dot{\gamma}^2$.

Under steady uniaxial extension, we calculate the fractional extension $\langle X_{bb} \rangle / L$, extensional viscosity η_e and first normal stress difference N_1 across a range of Wi values. Under steady shear flow, we calculate the fractional extension in x , y and z directions ($\langle X_{bb} \rangle / L$, $\langle Y_{bb} \rangle / L$, $\langle Z_{bb} \rangle / L$), first normal stress coefficient (ψ_1), shear viscosity η , orientation angle θ , and tumbling frequency ($\omega\tau_R$) over a range of Wi values. We use the radius of gyration along the flow and gradient directions to calculate the orientation angle θ to measure the alignment of the chains in the xy plane using the following equation [65].

$$\tan(2\theta) = \frac{2R_{g,xy}}{R_{g,xx} - R_{g,yy}} \quad (7)$$

To quantify and analyze the tumbling dynamics of the polymers under shear flow, we track and analyze the evolution of the angle between the end-to-end vector of the polymer chains and the x -axis, similar to the work of Dalal et. al. [66]. We monitor the angle as it progresses through the four quadrants of a full 360° rotation cycle and record the time taken for the chains to complete each full cycle (i.e., one complete rotation through all four quadrants) throughout the simulation and use the mean value as the tumbling time. We calculate tumbling frequency as inverse tumbling time, normalized by the relaxation time (τ_R).

III. RESULTS

A. Polyrotaxanes: Steady Uniaxial Extensional Flow

At the lower end of Wi range, the behavior of polyrotaxanes diverges significantly from linear polymers.

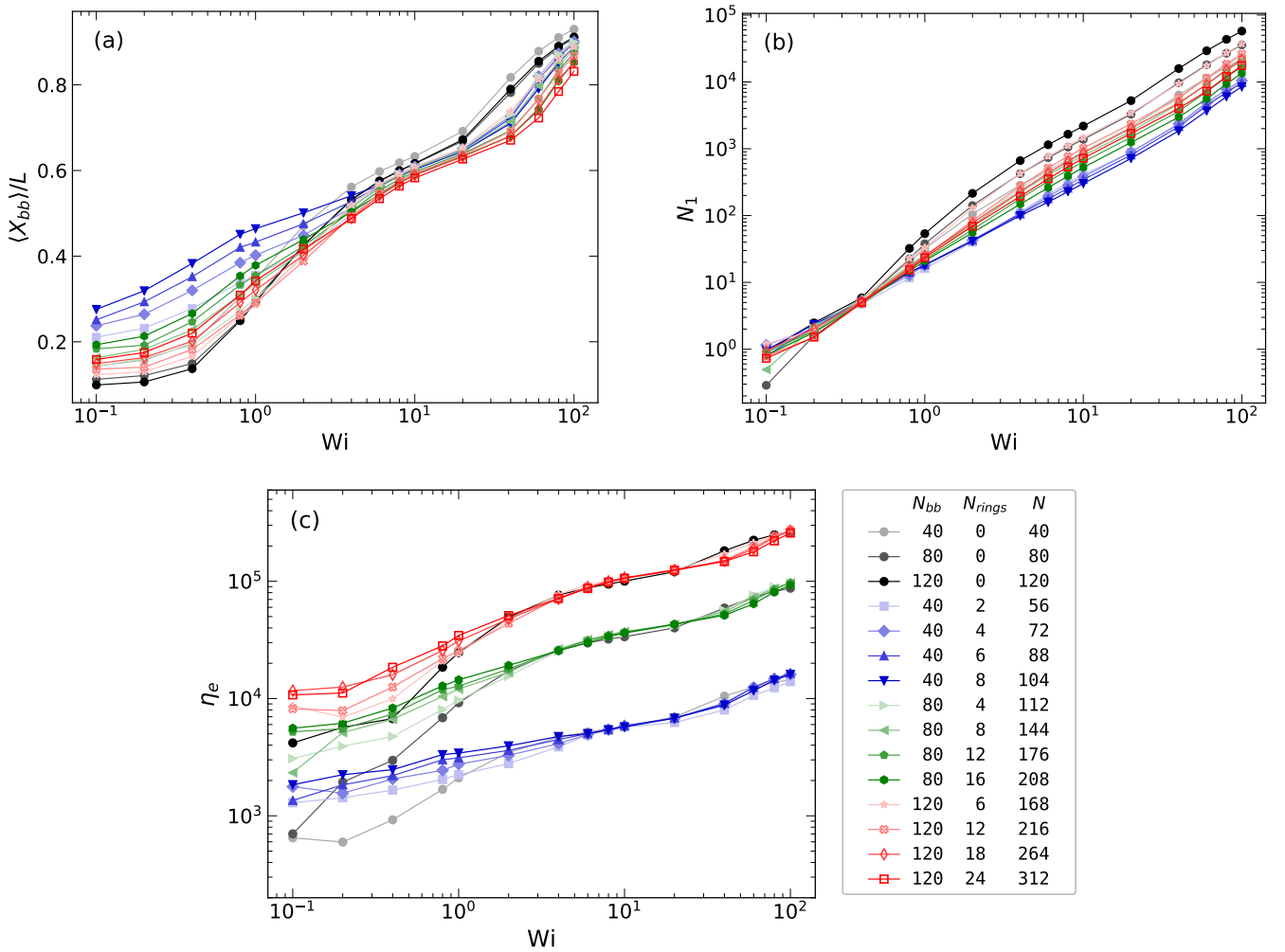


FIG. 2: Polyrotaxanes properties in extensional flow as a function of Weissenberg number (Wi): (a) fractional extension in flow direction ($\langle X_{bb} \rangle / L$), (b) first normal stress difference (N_1), (c) extensional viscosity (η_e). Linear polymers are shown in shades of gray with darker shades indicating more beads. Polyrotaxanes with 40, 80, and 120 backbone beads (N_{bb}) are shown in blue, green, and red, respectively; darker shades indicate higher ring density (N_{rings}/N_{bb}). The rings in the polyrotaxanes are composed of 8 beads, regardless of backbone length.

Fig. 2a shows adding rings to linear polymers increases $\langle X_{bb} \rangle / L$. This can be explained by the repulsive interactions between ring beads and backbone beads. These forces prevent backbone collapse, maintaining an extended conformation even in weak flows. Comparatively, linear polymers adopt more collapsed configurations in weak flows because of the lack of rings preventing collapse. At higher Wi values, the difference becomes negligible as both linear and polyrotaxane polymers reach fully extended backbone configurations.

The first normal stress difference (N_1) is lower in polyrotaxanes than linear polymers across the range of simulated Wi values, as shown in Fig. 2b. molecules with higher number of rings show lower (N_1) values. This can be related to the rings sliding over the backbone, leading to stress dissipation, resulting in less stress buildup in the flow direction. This shows polyrotaxanes have more pro-

nounced viscous and weaker elastic behavior compared with linear polymers without mechanical links. The mobile rings decrease the stress response of polyrotaxanes compared to linear counterparts.

As shown in Fig. 2c, at low Wi , polyrotaxanes show higher extensional viscosity (η_e) compared to linear polymers, with higher number of rings threaded in the backbone resulting in higher η_e . The higher η_e can be attributed to the stiffening effect of the rings on the backbone, causing the chains to be in a more extended configuration than a chain without rings. As a result, the polyrotaxanes have higher resistance to further elongation. At higher Wi values, the η_e difference between polyrotaxanes and linear polymers becomes less noticeable because all chains reach a relatively extended configuration and the rings do not play a significant role in the backbone conformation and resistance to extension.

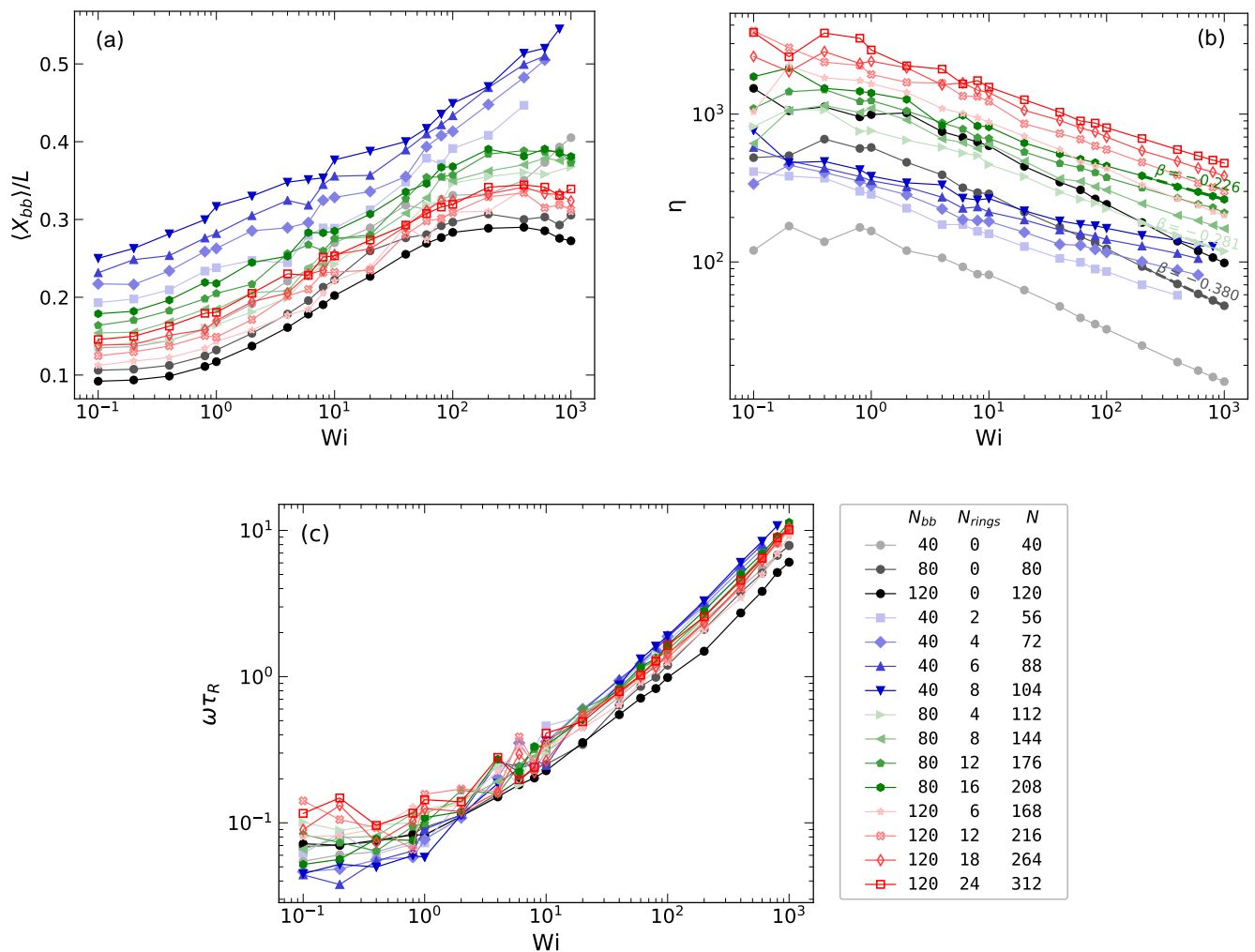


FIG. 3: Polyrotaxane properties in shear flow as a function of Weissenberg number (Wi): (a) fractional extension in flow direction ($\langle X_{bb} \rangle / L$), (b) shear viscosity (η), and (c) tumbling frequency ($\omega \tau_R$). Linear polymers are shown in shades of gray with darker shades indicating more beads. Polyrotaxanes with 40, 80, and 120 backbone beads (N_{bb}) are shown in blue, green, and red, respectively; darker shades indicate higher ring density (N_{rings}/N_{bb}). The rings in the polyrotaxanes are composed of 8 beads, regardless of backbone length.

B. Polyrotaxanes: Steady Shear Flow

Polymers in shear flow undergo continuous stretch-tumble cycles [67–69] and the fractional extension values reported in this work are averaged over those cycles. According to Fig. 3a, fractional extension in flow direction ($\langle X_{bb} \rangle / L$) in polyrotaxanes is higher than the linear polymers with the same number of backbone beads across the complete Wi range tested. Greater number of rings result in higher extension and more deviation from linear polymers. Overall, the repulsive ring-backbone interactions cause the molecules to exhibit extended configurations, which results in comparatively higher extension in flow direction.

A similar pattern is observed in $\langle Y_{bb} \rangle / L$ and $\langle Z_{bb} \rangle / L$, as shown in Fig. B.1a and Fig. B.1b. The presence of

rings in the polyrotaxanes increase the polymer’s extent in both the gradient (y) and cross-flow (z) directions, leading to greater fractional extension values compared to linear chains without rings. This occurs because the rings effectively increase the overall spatial span of the polymer. According to Fig. B.3c, the orientation angle (θ) in polyrotaxanes follows a trend similar to linear polymers, showing that the threaded rings have minimal effect on polymer orientation.

Polyrotaxanes exhibit higher shear viscosity (η) than their linear counterparts, with a larger number of threaded rings leading to a further rise in viscosity, as shown in Fig. 3b. The increase in viscosity of polymer solutions with increasing molecular weight is a well-established relationship in polymer science [70]. Thereby, it is not surprising to observe adding rings to a linear chain increase the viscosity as the molecular weight is

increased. In addition, rings limit the mobility of the chain, increasing the stress needed to deform the polymer from an extended configuration to induce tumbling. The power-law exponent β is lower in polyrotaxanes, where higher number of rings have lower β values. For example, a linear polymer with 80 beads has $\beta = -0.380$ whereas threading 4 or 16 rings to it decreases the β value to -0.281 and -0.226 , respectively, showing that polyrotaxanes have weaker shear thinning behavior which is caused by restricted segmental mobility under shear deformation caused by the rings.

In weak flow ($Wi \leq 1$), shear forces are not sufficient to induce significant tumbling in either polyrotaxanes or linear polymers, as shown in Fig. 3c. Consequently, both polymers have flat tumbling frequency profiles. As the flow strength increases ($1 < Wi < 10$), polyrotaxanes start to show enhanced tumbling compared to the linear counterparts. At $Wi \geq 10$, the threaded rings amplify the tumbling of the polyrotaxanes, causing significantly higher tumbling frequency compared with linear polymers. At $Wi = 800$, polyrotaxanes with 40 and 80 backbone beads (with 8 and 16 threaded rings, respectively) exhibit tumbling frequencies 38% and 35% higher than their linear polymer counterparts. Furthermore, within polyrotaxanes, threading more rings on a backbone increases the tumbling frequency. For instance, at $Wi = 1000$, a polyrotaxane with 80 beads in the backbone and 16 threaded rings tumbles 14% more frequently than one with only 4 rings. The enhanced tumbling in polyrotaxanes can be explained by the threaded rings increasing the polymer's hydrodynamic cross-section along the gradient direction. The expanded profile exposes a larger surface area to shear forces of the solvent, leading to greater torque and consequently, more frequent tumbling events.

C. Daisy Chains: Steady Uniaxial Extensional Flow

From Fig. 4a, at low Wi in extensional flow, daisy chains and linear polymers have similar fractional extension in flow direction $\langle X_{bb} \rangle / L$. In stronger flows, daisy chains start to diverge from linear chains and show less extension. For example, a daisy chain with 8 beads per segment and 6 segments ($M_w = 118$) extends 55% less than a comparable linear polymer ($M_w = 120$). The difference is less significant when the daisy chain contains longer linear segments. For example, the extension of daisy chains with 2 segments increases when beads per segment is increased from 8 to 16 and then to 32 (cold to hot colored curves), approaching the linear polymer behavior. Comparing daisy chains with the same length of linear segment and varying number of segments, shows that increasing the number of segments decreases the fractional extension, causing the chain to behave less like a linear polymer. This is due to higher fraction of the beads being in ring form, which is less extensible than a

linear segment. Overall, shorter linear segments or more linear segments in a daisy chain results in more deviation from a linear polymer, resulting in lower fractional extension.

As Fig. 4b shows, at low Wi , first normal stress difference (N_1) values are close in linear and daisy chains. At higher Wi values, daisy chains have lower N_1 values compared with linear polymers with the same molecular weight. This can be explained by stress dissipation through the mobile mechanical interlocks in the daisy chains. Also, comparing a daisy chain with 8 beads per segment and 4 segments to a chain with 32 beads per segment and 2 segments, which have comparable molecular weights of 74 and 78 respectively, shows that having shorter or more sections leads to lower N_1 values (at $Wi = 10$, the former yields $N_1 = 577$, whereas the latter reaches a higher value of $N_1 = 1548$).

Extensional viscosity (η_e) follows a similar trend as N_1 , as shown in Fig. 4c. Daisy chains exhibit lower extensional viscosity (η_e) than linear polymers of equivalent molecular weight. For example, at $Wi = 10$, a daisy chain with 32 beads per segment and 2 segments ($M_w = 78$) has 67% lower η_e compared to a linear polymer with 80 beads. The difference is more pronounced in daisy chains with shorter or more segments. A daisy chain with 8 beads per segment and 6 segments ($M_w = 118$) has 10 times lower η_e than a linear polymer with 120 beads. As an interesting example, at $Wi = 20$, a daisy chain with 16 beads per segment and 2 segments ($M_w = 46$) has 55% lower extensional viscosity than a linear polymer with $M_w = 40$, despite having 10% higher molecular weight. The same trend is evident at lower Wi values, although to a lesser extent. Overall, mechanical bonds in daisy chains lower extension, stress and η_e .

D. Daisy Chains: Steady Shear Flow

As shown in Fig. 5a, fractional extension in the flow direction has different regimes based on Wi number. At $Wi < 0.8$, $\langle X_{bb} \rangle / L$ remains nearly constant in linear polymers and daisy chains. At higher Wi , the fractional extension increases and then decreases around $Wi \approx 10^2$. While the conformational change is seen in both linear and daisy chains, the variation is much less significant in daisy chains with shorter or more segments. For example, a daisy chain with 8 beads per segment and 10 segments shows a nearly constant fractional extension across the whole Wi range with minimal variation, while decreasing the number of segments increases the variation. Also, in daisy chains with the same number of segments, longer segments result in behavior similar to a linear polymer. A terminal increasing regime is seen at very high Wi in linear polymers. However, this behavior could not be confirmed in daisy chains because with our current model, the chains disentangle under very strong flow conditions. We plan to address this shortcoming in future work.

According to Figs. B.2a and B.2b, fractional exten-

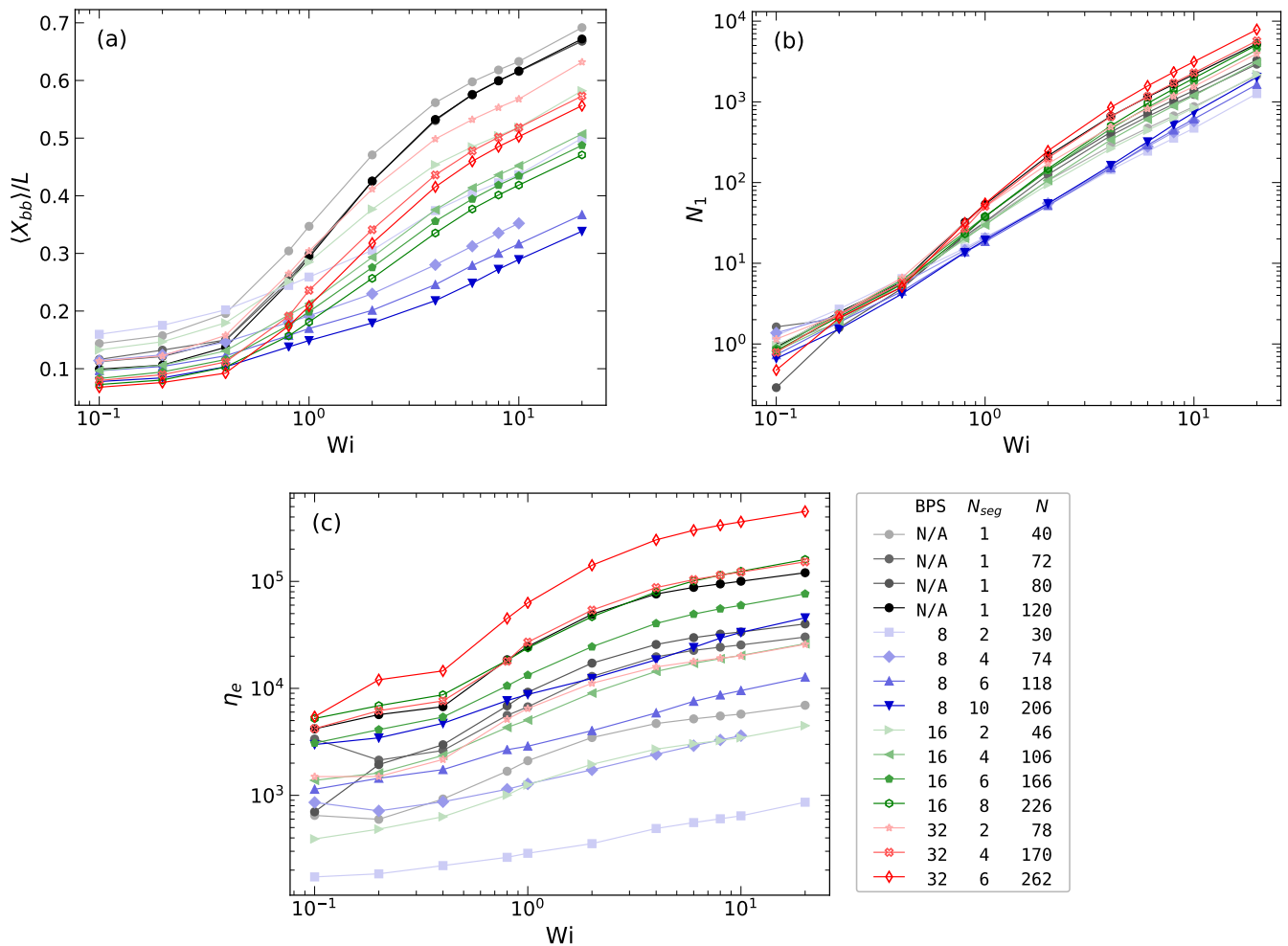


FIG. 4: Daisy chain properties in extensional flow as a function of Weissenberg number (Wi): (a) fractional extension in flow direction ($\langle X_{bb} \rangle / L$), (b) first normal stress difference (N_1), (c) extensional viscosity (η_e). Linear polymers are shown in shades of gray with darker shades indicating more beads. Daisy chains with 8, 16, and 32 beads per segment (BPS) are shown in blue, green, and red, respectively; darker shades indicate more segments (N_{seg}). The rings in all daisy chains are composed of 8 beads.

sions in the gradient and cross directions show a similar constant regime at low Wi followed by a decreasing regime at higher Wi . Similar to flow direction, $\langle Y_{bb} \rangle / L$ and $\langle Z_{bb} \rangle / L$ show less variation in daisy chains with shorter or more segments. $\langle Z_{bb} \rangle / L$ in daisy chains exhibit an increasing terminal regime corresponding to the decrease in $\langle X_{bb} \rangle / L$, but we could not confirm this in all daisy chains due to model limitations. As shown by the orientation angle in Fig. B.2c, daisy chains exhibit little orientation in weak flows and reach their peak orientation angle at $Wi \approx 7$, compared to $Wi \approx 3$ for linear polymers, indicating that a stronger flow is needed to align daisy chains. This can be attributed to rearrangements at the mechanical bonds. At high Wi , linear polymers reach a small angle of $\approx 2^\circ$, while daisy chains of equal molecular weight maintain a higher angle of $\approx 4.5^\circ$, reflecting differences in aspect ratio discussed in the tumbling dynamics

section.

Fig. 5b shows that the daisy chains are shear thinning polymers similar to linear polymers, with shear viscosity decreasing with Wi . However, the power-law exponent is lower in daisy chains with shorter or more segments, deviating from linear polymers. For example, a daisy chain with 8 beads per segment and 6 segments ($M_w = 118$) has $\beta = -0.225$ while the corresponding linear polymer ($M_w = 120$) has $\beta = -0.390$, which shows the less pronounced shear-thinning character of the daisy chains. This daisy chain has significantly lower viscosity as well, highlighting another major deviation from the linear polymers. For instance, at $Wi = 20$, a daisy chain with 32 beads per segment and 2 segments ($M_w = 78$) has 42% lower viscosity than the corresponding linear polymer ($M_w = 80$). It is worth noting that due to the difference in shear-thinning degree between linear and

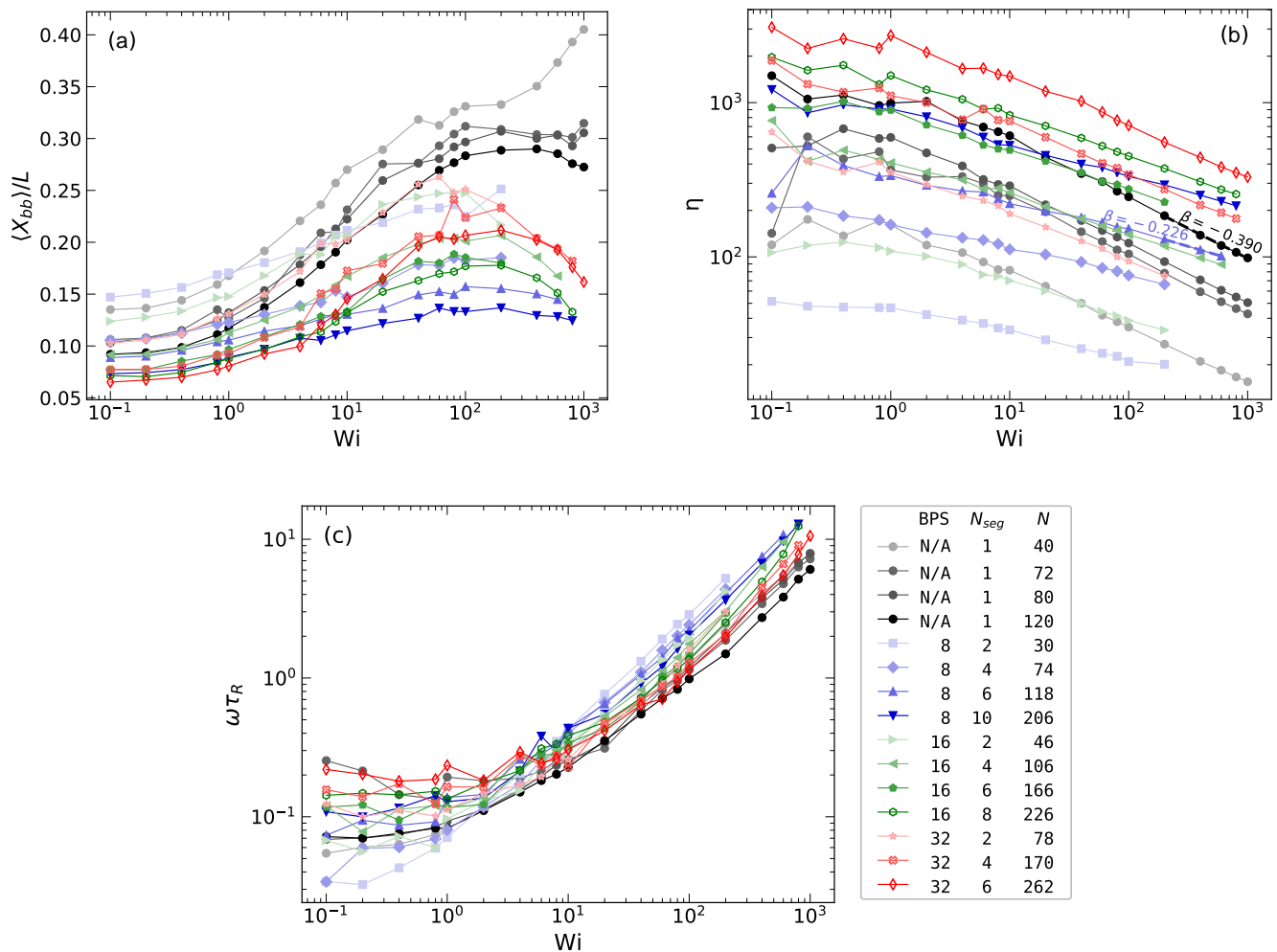


FIG. 5: Daisy chain properties in shear flow as a function of Weissenberg number (Wi): (a) fractional extension in flow direction ($\langle X_{bb} \rangle / L$), (b) shear viscosity (η), and (c) tumbling frequency ($\omega \tau_R$). Linear polymers are shown in shades of gray with darker shades indicating more beads. Daisy chains with 8, 16, and 32 beads per segment (BPS) are shown in blue, green, and red, respectively; darker shades indicate higher number of segments (N_{seg}). The rings in all daisy chains are composed of 8 beads.

daisy chain polymers, the viscosity difference is more pronounced in weaker flows and diminishes in stronger flows. As an example, a daisy chain with 8 beads per segment and 6 segments ($M_w = 118$) has 520% lower viscosity than the comparable linear polymer ($M_w = 120$) at $Wi = 0.1$ but the difference decreases at $Wi = 600$ to a less significant value of 27%.

Based on Fig. 5c, at low Wi , the flow is not strong enough to cause significant tumbling in either the daisy chains or linear polymers. At higher Wi , daisy chains show significantly more frequent tumbling in shear flow. At $Wi = 200$, a daisy chain with 8 beads per segment and 6 segments ($M_w = 118$) shows 87% higher $\omega \tau_R$ than a linear polymer with 120 beads. Similarly, a daisy chain with 32 beads per segment and 2 segments ($M_w = 78$) has 60% higher $\omega \tau_R$ than the linear counterpart with 80 beads. In shear flow, the greater extent of polymers in

the gradient direction causes larger shear forces from the flow to be applied to the chains, resulting in more frequent tumbles. The rings in the daisy chains increase the gradient-flow extent. This effect is less present in configurations with fewer or longer segments, making them more linear-like in terms of aspect ratio, showing less tumbling. On the other hand, the role of the rings in the aspect ratio is more pronounced in daisy chains with more or shorter segments, causing the chains to experience larger shear forces from the flow, resulting in higher tumbling frequency. In addition to aspect ratio, the mechanical interlocks make the polymer structure more flexible, further enhancing tumbling.

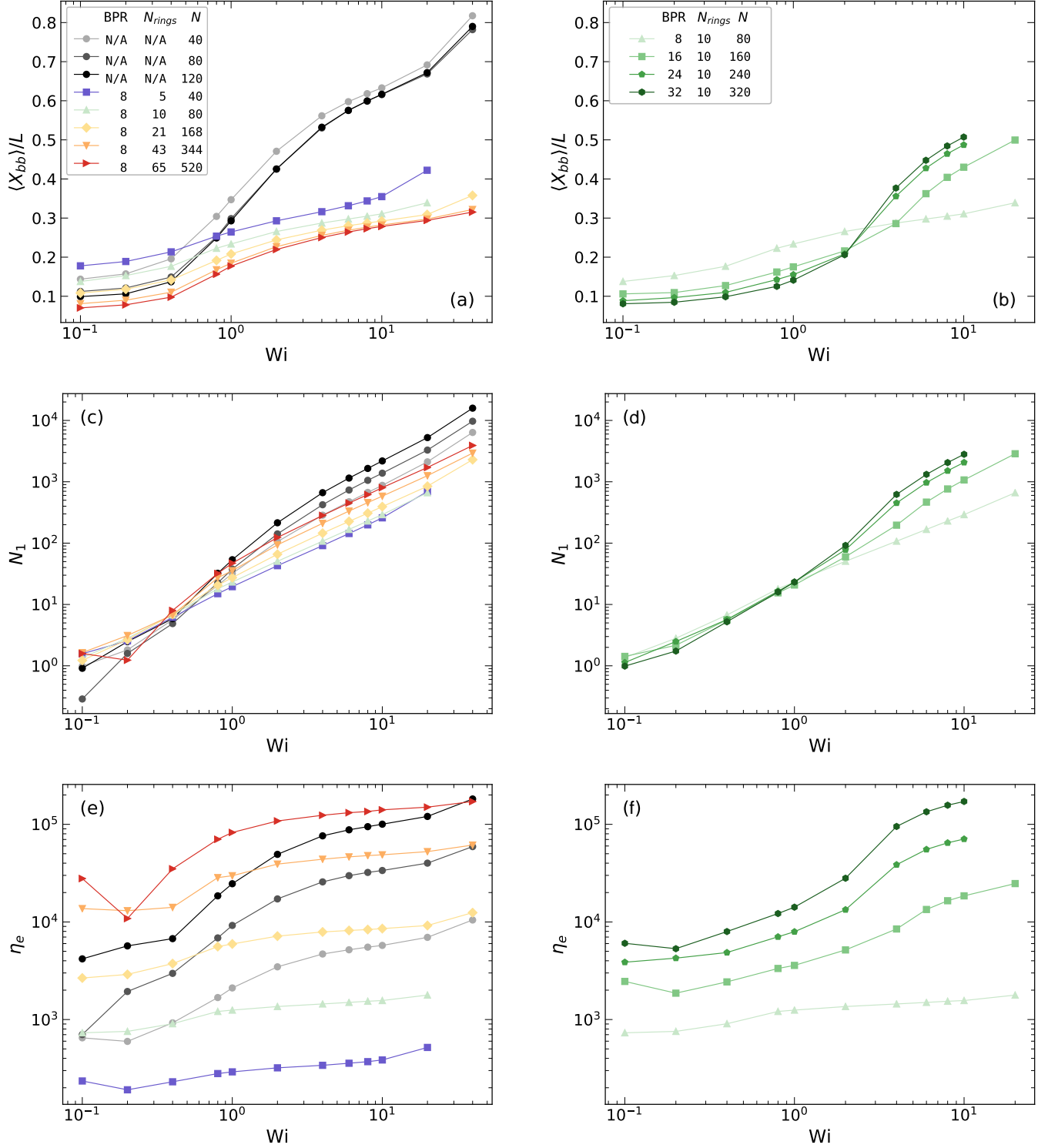


FIG. 6: Polycatenane properties in extensional flow as a function of Weissenberg number (Wi): (a, b) fractional extension in flow direction ($\langle X_{bb} \rangle / L$), (c, d) first normal stress difference (N_1), (e, f) extensional viscosity (η_e). Linear polymers are shown in shades of gray with darker shades indicating more beads. Colors from cold to hot indicate higher number of rings (N_{rings}) with fixed beads per ring (BPR = 8). Darker shades of green indicate increasing beads per ring (BPR) in polycatenanes with fixed number of rings ($N_{rings} = 10$).

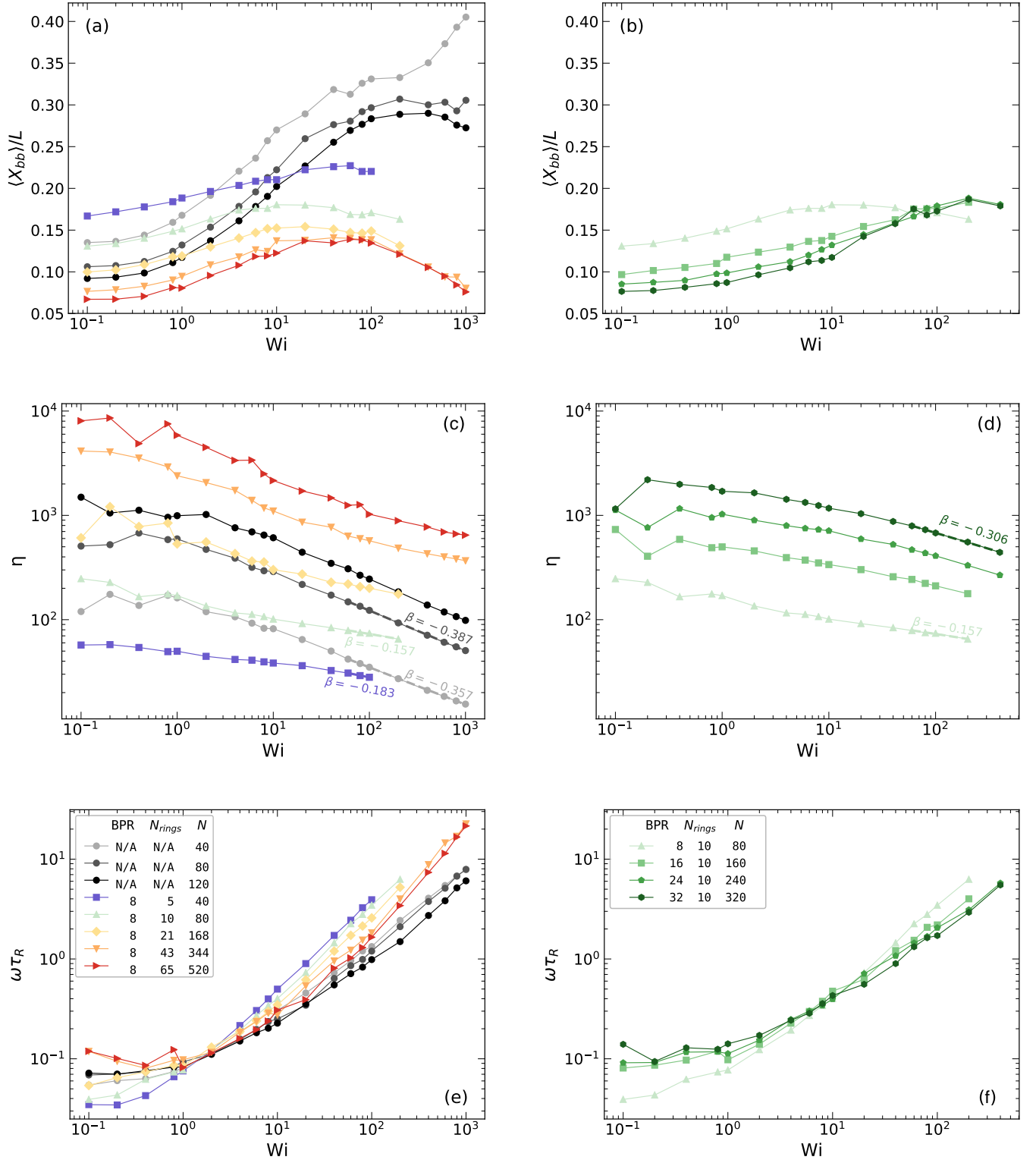


FIG. 7: Polycatenane properties in shear flow as a function of Weissenberg number (Wi): (a, b) fractional extension in flow direction ($\langle X_{bb} \rangle / L$), (c, d) shear viscosity (η), (e, f) tumbling frequency (ω_{TR}). Linear polymers are shown in shades of gray with darker shades indicating more beads. Colors from cold to hot indicate higher number of rings (N_{rings}) with fixed beads per ring (BPR = 8). Darker shades of green indicate increasing beads per ring (BPR) in polycatenanes with fixed number of rings ($N_{rings} = 10$).

E. Polycatenanes: Steady Uniaxial Extensional Flow

Fig. 6a shows the fractional extension of polycatenanes in flow direction. At low Wi , $\langle X_{bb} \rangle / L$ is higher in polycatenanes than linear polymers with the same number of beads. This stems from steric repulsions between interlocked rings, which enforce elongated conformations, compared with the equilibrium coiled state of linear polymers. However, at medium to high Wi , linear polymers become more extended than polycatenanes because repulsion between and within catenane rings hinders further elongation. In contrast, linear polymers uncoil and extend readily. Decreasing the number of rings increases $\langle X_{bb} \rangle / L$ because fewer rings minimize overlap, allowing the chain to approach the maximum extension of a linear chain with $N_{bb}/2$ beads. Interestingly, variation in $\langle X_{bb} \rangle / L$ is less in polycatenanes that have fewer rings. For instance, a polycatenane with 8 beads per ring and 5 rings extends only 2 times beyond equilibrium, while a polycatenane chain with the same ring size and 65 rings stretches over 3 times. This is because more rings give the chain more degrees of freedom. This can be better understood by assuming each ring a repeat unit. More repeat units in a chain makes it more flexible. In the limiting case, if we continue increasing the number of rings indefinitely, the chain approaches a linear polymer [71].

As shown in Fig. 6b, increasing the ring size while keeping the number of rings constant leads to more variability of $\langle X_{bb} \rangle / L$ because the beads in the same ring experience less repulsions until they become fully extended. The chains with larger rings have more flexibility [33] and can collapse and extend more readily. As a result, in weak flows, chains with smaller rings exhibit higher $\langle X_{bb} \rangle / L$, whereas in strong flows, chains with larger rings show greater extension.

According to Fig. 6c, at low Wi , polycatenanes have higher (N_1) than linear polymers with the same molecular weight because the interlocks prevent chain collapse and increase stress buildup. At medium to high Wi , linear polymers are more extended and have higher (N_1) . Furthermore, (N_1) increases with increasing number of rings and ring size primarily due to higher M_w . Furthermore, (N_1) increases with increasing number of rings primarily due to higher M_w . Increasing ring size has a similar effect, as evident from Fig. 6d.

Extensional viscosity (η_e) is significantly lower in polycatenanes compared to linear polymers with the same molecular weight, as shown in Fig. 6e. For instance, a polycatenane with 8 beads per ring and 10 rings ($M_w = 80$) has 22 times lower (η_e) than a linear polymer with 80 beads at $Wi = 10$. Furthermore, adding more rings to a polycatenane increases the extensional viscosity due to increased molecular weight of the polymers. The same effect is achieved by making the rings larger, as seen in Fig. 6f. Comparing a polycatenane with 16 beads per ring and 10 rings ($M_w = 160$) to a polycatenane with 8 beads per ring and 21 rings ($M_w = 168$) allows us to de-

couple the effects of molecular weight from the impact of chain topology on viscosity. Based on Figs. 6e and 6f, at low Wi , the chain with more small rings has higher viscosity. This reflects the more extended conformation of the smaller rings, leading to higher stress and resistance to extension. At high Wi , the chain with fewer large rings show significantly higher extensional viscosity, up to 270% higher at the highest Wi . Under strong extensional flow, the rings in the chain with fewer large rings are more effectively stretched, leading to an increased resistance to further deformation. The extended conformation under high strain produces a larger stress response, which is reflected in the higher measured extensional viscosity. In contrast, the greater number of flexible mechanical interlocks in the chain with more small rings facilitates stress relaxation when subjected to high strain rates. This relaxation mechanism ultimately reduces η_e relative to the chain with fewer large rings.

F. Polycatenanes: Steady Shear Flow

As shown in Fig. 7a, at low Wi , $\langle X_{bb} \rangle / L$ remains nearly constant in polycatenanes as the flow is not strong enough to create significant deformation in the chains. For $1 \leq Wi \leq 100$, there is a regime with increasing extension which corresponds to chains being extended in flow direction. In chains with 21 or more rings, there is a decreasing regime in the $100 \leq Wi$ range. This corresponds to expansion in cross-flow direction. This behavior could not be verified in chains with 5 and 10 rings because the chains could not withstand the strength of the flow and dethreaded. At low Wi , $\langle X_{bb} \rangle / L$ is higher in polycatenanes than linear polymers with the same molecular weight due to entangled ring topologies leading to strong repulsive interactions, keeping the chains more extended. At higher Wi , linear polymers become more extended in flow direction than the polycatenanes. This is because the linear polymers are free to change conformation from coiled to stretched states in the flow, while the rings in polycatenanes have steric constraints, preventing them from significant deformation. In addition, mechanical interlocks limit the extension of the chains due to inter-ring repulsion. Chains with fewer rings have limited variation of $\langle X_{bb} \rangle / L$ throughout the Wi range, while chains with higher number of rings can be deformed more readily in the flow, leading to larger variation of fractional extension in flow direction. In addition, higher number of rings leads to lower fractional extension as the chains are more flexible and can relax to a coiled state. Based on 7b, increasing the ring size has the same effect on $\langle X_{bb} \rangle / L$ at low to medium Wi . At high Wi , the effect becomes negligible.

Figs. B.3a and B.3b show that $\langle Y_{bb} \rangle / L$ and $\langle Z_{bb} \rangle / L$ are higher in polycatenanes than linear polymers because the rings add extra span in those directions, while increasing ring size or adding more rings decrease the extensions primarily due to the normalization factor effects. $\langle Y_{bb} \rangle / L$

and $\langle Z_{bb} \rangle / L$ show a decreasing regime, while $\langle Z_{bb} \rangle / L$ decreases only up to $Wi = 100$ after which an increasing regime is evident corresponding to decreasing $\langle X_{bb} \rangle / L$. According to Fig. B.3c, at low Wi polymers remain unaligned. At moderate Wi , the orientation angle θ first rises then falls, with polycatenanes of 8 beads per ring exhibiting a secondary increase previously noted in other systems [44]. A terminal decrease, reflecting alignment with very strong flow, could not be verified here because chains broke at high Wi . Having more or smaller rings shifts the primary peak to higher Wi and brings the secondary rise to lower Wi . Having more or larger rings make the orientation angle approach that of a linear polymer.

Polycatenanes show significantly lower shear viscosity than linear polymers, as shown in Fig. 7c. For example at $Wi = 10$, the viscosity of a polycatenane with 8 beads per ring and 10 rings ($M_w = 80$) is 35% of the linear polymer with 80 beads. This is due to the larger polymer extent in gradient direction which creates larger shear forces and larger deformation. In addition, viscosity varies less in the polycatenanes across the simulated Wi range compared with linear polymers. The power-law exponent for polycatenanes is 50% less than the linear polymers at the same molecular weight, suggesting weaker shear-thinning behavior. This can be understood by the fact that in linear polymers, higher shear rates cause the polymers to uncoil, extend, and align with the flow, leading to a significant decrease in viscosity. In contrast, polycatenanes do not deform, coil, or uncoil as readily under shear due to the repulsive interactions inherent in their interlocked structure, resulting in a flatter viscosity profile and less sensitivity to changes in shear rate. Increasing the number of rings in polycatenanes leads to a higher viscosity, primarily because of the increase in molecular weight. The slope of the viscosity curve increases as well. This is due to enhanced flexibility, leading to more prominent coiling and uncoiling, which leads to stronger shear-thinning properties. According to Fig. 7d, increasing the ring size has a similar effect, leading to higher shear viscosity and enhanced shear-thinning behavior.

At very low Wi number, polycatenanes have decreased tumbling frequency compared to linear polymers, as shown in Fig. 7e. This is due to higher polymer extent in flow direction, creating greater moment of inertia, making it more difficult for a weak flow to rotate the chain. However, because of the interlocked rings, polycatenanes are thicker in gradient direction, making them more responsive to the flow strength. As a result, a slight increase in Wi causes more tumbling in polycatenanes compared with linear polymers, where tumbling frequency remains fairly constant in low Wi regime. At moderate to high Wi number, polycatenanes tumble more efficiently than linear polymers. For instance, at $Wi = 200$, a polycatenane with 8 beads per ring and 10 rings ($M_w = 80$) tumbles 3 times more frequently than the linear polymer with 80 beads. Additionally, more

rings in a polycatenane decreases tumbling frequency at moderate to high Wi number. This can be explained by the resulting increase in aspect ratio of the polymer, making the polymer thickness less effective, causing the chains to behave more like linear polymers. Increasing the ring size has a similar effect on tumbling frequency, as shown in Fig. 7f. This can be understood by the increased degrees of freedom at the mechanical interlocks, which allows the rings to rotate freely against each other and dissipate the shear stress, leading to lower tumbling frequency of the polymer.

IV. DISCUSSION

The presence of mechanical bonds gives rise to notable quantitative differences compared with linear polymers. Unlike linear polymers that coil under weak flow, in polyrotaxanes, ring-backbone repulsion causes more extended equilibrium configurations and earlier chain extension in flow. Polyrotaxanes show lower normal stress difference and weaker elasticity due to stress relief from sliding rings. Extensional viscosity is higher in polyrotaxanes especially in shorter chains with more rings due to increased stiffness and resistance to elongation. Under shear flow, polyrotaxanes extend more in all directions and have higher viscosity, with reduced shear thinning, as the rings limit mobility, requiring more stress for deformation. In addition, tumbling frequency is higher and it increases with number of rings due to enhanced hydrodynamic cross-section from threaded rings.

Daisy chains extend less than linear polymers and have lower normal stress difference, extensional and shear viscosity. They tumble more frequently at high Wi , due to higher gradient-direction extent and aspect ratio effects with more or shorter segments pronouncing these effects, causing greater deviation from linear polymers.

Polycatenanes are less extended and have lower first normal stress difference than linear chains except at very low Wi . They lack the smooth transition from coiled to stretched states typical of linear polymers. Polycatenanes show significantly lower extensional and shear viscosities, as well as weaker shear thinning. More or larger rings in polycatenanes increases viscosity, primarily due to increased molecular weight. Polycatenanes tumble more frequently, with fewer or smaller rings enhancing this effect.

Overall, the interlocked topology of each MIP leads to a distinct set of rheological properties, as illustrated in Fig. 8. Here we give an example of each polymer type, all with a similar molecular weight. We compare polymer types with similar maximum contour lengths (L) in Fig. B.5. For a given molecular weight, we see that in both extensional (Fig. 8a) and shear flow (Fig. 8c), polyrotaxanes exhibit the greatest relative stretch in the flow direction because of their linear backbone and large cross-flow extent due to their rings. The daisy chain and the polycatenane are relatively unextended because of the

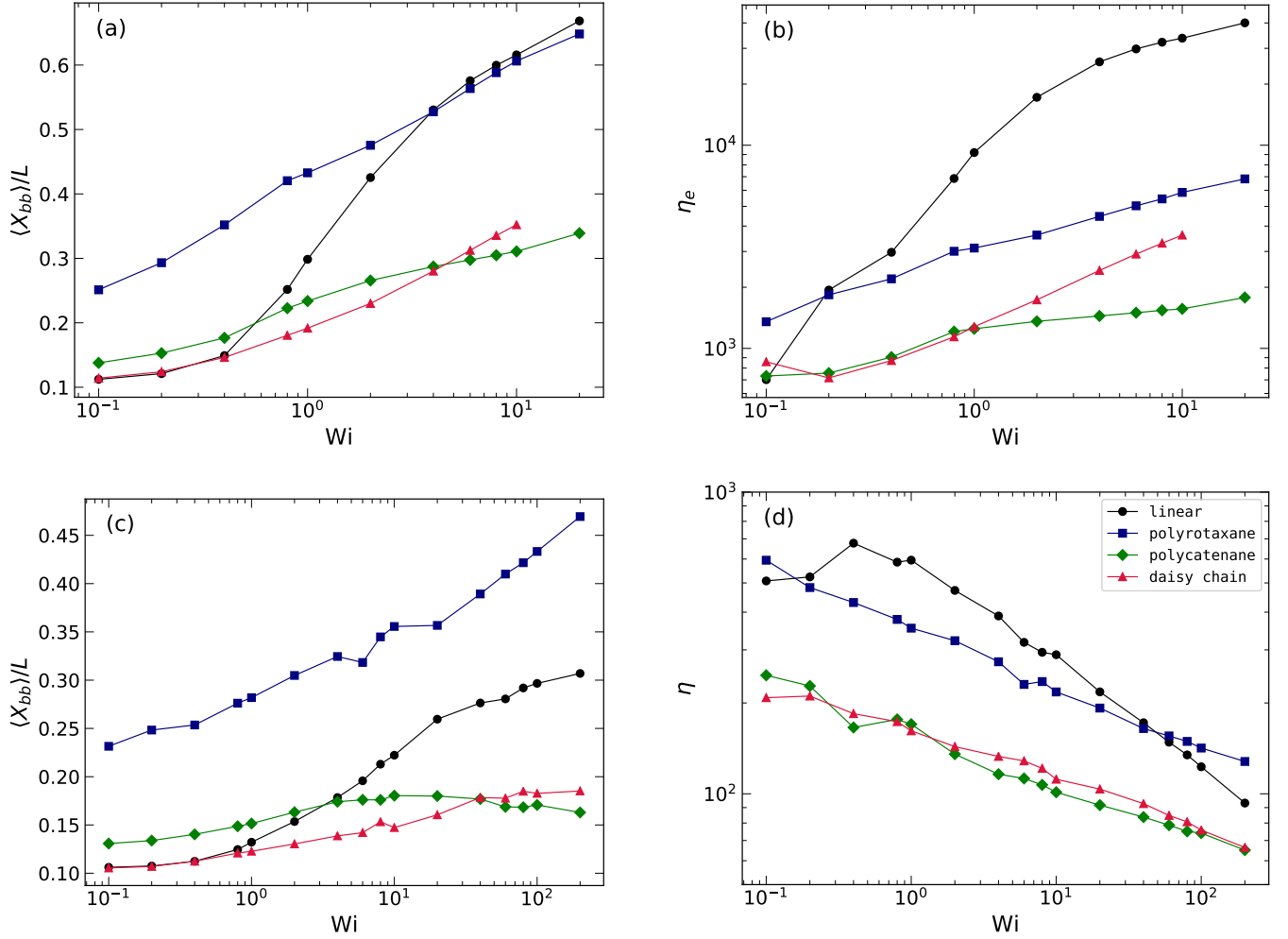


FIG. 8: Comparison of linear and MIP polymers of similar molecular weight in extensional (a, b) and shear (c, d) flow. Fractional extension in the flow direction ($\langle X_{bb} \rangle / L$) for extension (a) and shear (c) along with extensional viscosity (η_e) (b) and shear viscosity (η) are given as a function of Weissenberg number (Wi). The linear polymer (black) has 80 backbone beads ($M_w = 80$). The polyrotaxane (blue) has 40 backbone beads including 2 capping beads and 6 rings ($M_w = 88$). The daisy chain (green) has 4 linear segments of 8 beads each interlocked with 6 8 bead rings ($M_w = 74$) and includes 2 capping beads. The polycatenane (red) has 10 interconnected rings of 8 beads each $M_w = 80$.

lower extensibility of rings and their resistance to overlap. This leads to fairly consistent stretch of the daisy chain and the polycatenane across a wide range of Wi, varying only between 0.10 and 0.37 in extension and 0.09 and 0.18 in shear, much lower variability than other two polymer types. For a given molecular weight, the polymers also exhibit variation in their viscosity. In extensional flow, the linear polymer has the greatest extensional viscosity for all but the lowest Wi range, as seen in Fig. 8b. The mechanical bonds in all MIP types lead to lower extensional viscosity, with the daisy chain behaving similar to the linear polymer and the polyrotaxane and polycatenane showing weaker scaling of their extensional viscosity than the linear polymer and daisy chain. In shear flow (Fig. 8d), the linear polymer has higher shear viscosity

than the MIPs except the polyrotaxane, which overtakes the linear polymer at a cross-over around $Wi \approx 50$. This demonstrates the reduced shear thinning of the polyrotaxane. Indeed all of the MIPs' shear viscosity scales less strongly with Wi than the linear polymer, demonstrating that the mechanical bonds suppress shear-thinning behavior. Similar to extensional viscosity, the shear viscosity of the polycatenane is the lowest of all polymer types.

In line with the varied rheological responses that we have reported, MIPs have already shown their potential in a range of applications. Slide-ring gels, a category of polyrotaxanes in which mechanically interlocked rings function as movable cross-links, could potentially be used as protective coatings in automobiles and smartphones

due to their scratch-resistance and self-healing properties [72]. Olympic gels (materials formed entirely by interlocked rings) [73], which have been synthesized recently using over 16,000 DNA rings, exhibit unique non-linear elasticity and swelling behavior [74]. In addition, previous simulations of rotaxanes, slide-ring gels and tendomer gels in equilibrium and mechanical strain have demonstrated exceptional elasticity and yield stresses surpassing conventional cross-linked polymer gels [39, 40, 75–81]. Furthermore, the unusual physical characteristics of polysiloxanes along with the depolymerization behavior and elastic, rubber-like properties of polyphosphonitrilic chloride have been attributed to interlocked cyclic polymer structures [82, 83]. These examples demonstrate the unique properties imparted by mechanical bonds. Our results hint at additional potential uses of MIPs, as well. High molecular weight polymers are known to reduce drag in pipe flow [84–87], at least partially due to the suppression of vortex formation caused by extended polymer configurations. The lower shear viscosity for MIPs compared to typical linear polymers and the greater extension of polyrotaxanes in particular, then, suggest that MIPs could be developed into drag reducing agents. Similarly, extended polymers in liquid petroleum-based fuels favor the formation of larger droplets that are less prone to ignition during accidental fuel releases [88–90]. The greater extension of polyrotaxanes also suggests their potential development as mist-suppressing fuel additives to improve liquid fuel safety.

As a first step toward characterizing the flow behavior of mechanically interlocked polymers, this work provides valuable insights into their dynamics in dilute solutions under weak to moderate flow conditions. However, strong flow regimes remain unexplored as our current model fails to maintain polymer integrity at high Weissenberg numbers. Under such conditions, large hydrodynamic forces can cause the rings in all three MIP architectures to slip through the polymer backbone, or through each other in the case of polycatenanes. This degradation is consistent with experiments that demonstrate that rotaxanes undergo unstopping under high mechanical force [91]. Experimental observations also suggest that mechanical bonds in catenanes are comparable in strength to covalent bonds [92]. To fully capture degradation mechanisms in strong flow, future work will move beyond the FENE bond model and incorporate dissociable bonds, revealing combined chemical and mechanical modes of polymer failure. This future work will lead to a better understanding of the durability of MIPs in flow for potential engineering applications.

V. CONCLUSIONS

In this study, we explored how mechanical bonds affect the dynamics and rheology of dilute solutions of

mechanically-interlocked polymers under steady shear and uniaxial extension. We used a coarse-grained bead-spring model with excluded volume and hydrodynamic interactions in a Brownian dynamics simulation. To elucidate the effect of mechanical interlocks on properties, we ran a series of simulations across a range of flow strengths (Wi numbers) and polymer structures. In polyrotaxanes, the number of rings was varied. In daisy chains, the number and the length of the linear segments were varied. Lastly, in polycatenanes, the number of rings and their sizes were varied. Our simulations reveal that mechanical interlocks significantly alter polymer behavior under various flow conditions, with polyrotaxanes, daisy chains, and polycatenanes each exhibiting distinctive rheological signatures compared to linear polymers. This work provides a foundation for understanding MIP behavior in dilute solutions under weak to moderate flows. Addressing strong flow regimes and mechanical degradation mechanisms in future studies will help fully realize the potential of these novel materials.

ACKNOWLEDGMENTS

The authors gratefully acknowledge the financial support of Wayne State University and the computational resources of Wayne State University’s High Performance Computing. The authors also thank Charles Manke for valuable feedback and discussions.

SUPPLEMENTARY MATERIAL

The supplementary material includes the fractional extension in y and z directions, orientation angle, and first normal stress coefficient against Wi ; equilibrium properties of the polymers studied; comparison graphs of linear and MIPs with similar contour length.

AUTHOR DECLARATIONS

Conflict of Interest

The authors have no conflicts.

DATA AVAILABILITY

Data will be available in a persistent Zenodo repository. Simulation code is available at <https://github.com/albaugh/polymer>.

- [1] Hart, L. F.; Hertzog, J. E.; Rauscher, P. M.; Rawe, B. W.; Tranquilli, M. M.; Rowan, S. J. Material properties and applications of mechanically interlocked polymers. *Nature Reviews Materials* **2021**, *6*, 508–530.
- [2] Sluysmans, D.; Stoddart, J. F. The burgeoning of mechanically interlocked molecules in chemistry. *Trends in Chemistry* **2019**, *1*, 185–197.
- [3] Liu, G.; Rauscher, P. M.; Rawe, B. W.; Tranquilli, M. M.; Rowan, S. J. Polycatenanes: synthesis, characterization, and physical understanding. *Chemical Society Reviews* **2022**, *51*, 4928–4948.
- [4] Ando, S.; Ito, K. Recent Progress and Future Perspective in Slide-Ring Based Polymeric Materials. *Macromolecules* **2025**, *58*, 2157–2177.
- [5] Wu, Q.; Rauscher, P. M.; Lang, X.; Wojtecki, R. J.; De Pablo, J. J.; Hore, M. J.; Rowan, S. J. Poly [n] catenanes: Synthesis of molecular interlocked chains. *Science* **2017**, *358*, 1434–1439.
- [6] Harrison, I. T.; Harrison, S. Synthesis of a stable complex of a macrocycle and a threaded chain. *Journal of the American Chemical Society* **1967**, *89*, 5723–5724.
- [7] Wenz, G.; Keller, B. Threading cyclodextrin rings on polymer chains. *Angewandte Chemie International Edition* **1992**, *31*, 197–199.
- [8] Ashton, P. R.; Baxter, I.; Cantrill, S. J.; Fyfe, M. C.; Glink, P. T.; Stoddart, J. F.; White, A. J.; Williams, D. J. Supramolecular daisy chains. *Angewandte Chemie International Edition* **1998**, *37*, 1294–1297.
- [9] Wenz, G.; Han, B.-H.; Müller, A. Cyclodextrin rotaxanes and polyrotaxanes. *Chemical Reviews* **2006**, *106*, 782–817.
- [10] Schill, G.; Lüttringhaus, A. The preparation of catena compounds by directed synthesis. *Angewandte Chemie International Edition* **1964**, *3*, 546–547.
- [11] Frisch, H. L.; Wasserman, E. Chemical topology 1. *Journal of the American Chemical Society* **1961**, *83*, 3789–3795.
- [12] Weidmann, J.-L.; Kern, J.-M.; Sauvage, J.-P.; Muscat, D.; Mullins, S.; Köhler, W.; Rosenauer, C.; Räder, H. J.; Martin, K.; Geerts, Y. Poly [2] catenanes and cyclic oligo [2] catenanes containing alternating topological and covalent bonds: Synthesis and characterization. *Chemistry—A European Journal* **1999**, *5*, 1841–1851.
- [13] Segawa, Y.; Kuwayama, M.; Hijikata, Y.; Fushimi, M.; Nishihara, T.; Pirillo, J.; Shirasaki, J.; Kubota, N.; Itami, K. Topological molecular nanocarbons: All-benzene catenane and trefoil knot. *Science* **2019**, *365*, 272–276.
- [14] Leigh, D. A.; Pritchard, R. G.; Stephens, A. J. A Star of David catenane. *Nature Chemistry* **2014**, *6*, 978–982.
- [15] Araki, J.; Zhao, C.; Ito, K. Efficient production of polyrotaxanes from α -cyclodextrin and poly (ethylene glycol). *Macromolecules* **2005**, *38*, 7524–7527.
- [16] Cai, K.; Shi, Y.; Zhuang, G.-W.; Zhang, L.; Qiu, Y.; Shen, D.; Chen, H.; Jiao, Y.; Wu, H.; Cheng, C.; others Molecular-pump-enabled synthesis of a daisy chain polymer. *Journal of the American Chemical Society* **2020**, *142*, 10308–10313.
- [17] Datta, S.; Kato, Y.; Higashiharaguchi, S.; Aratsu, K.; Isobe, A.; Saito, T.; Prabhu, D. D.; Kitamoto, Y.; Hol-lamby, M. J.; Smith, A. J.; others Self-assembled polycatenanes from supramolecular toroidal building blocks. *Nature* **2020**, *583*, 400–405.
- [18] Gartner III, T. E.; Jayaraman, A. Modeling and simulations of polymers: a roadmap. *Macromolecules* **2019**, *52*, 755–786.
- [19] Li, Y.; Abberton, B. C.; Kröger, M.; Liu, W. K. Challenges in multiscale modeling of polymer dynamics. *Polymers* **2013**, *5*, 751–832.
- [20] Gedde, U. W.; Hedenqvist, M. S.; Hakkarainen, M.; Nilsson, F.; Das, O. *Applied Polymer Science*; Springer International Publishing: Cham, 2021; pp 205–265.
- [21] Seyedi, A.; Najafi, M.; Russell, G. T.; Mohammadi, Y.; Vivaldo-Lima, E.; Penlidis, A. Initiator feeding policies in semi-batch free radical polymerization: a Monte Carlo study. *Processes* **2020**, *8*, 1291.
- [22] Kremer, K.; Grest, G. S. Dynamics of entangled linear polymer melts: A molecular-dynamics simulation. *The Journal of Chemical Physics* **1990**, *92*, 5057–5086.
- [23] Rauscher, P. M.; Rowan, S. J.; de Pablo, J. J. Hydrodynamic interactions in topologically linked ring polymers. *Physical Review E* **2020**, *102*, 032502.
- [24] Bohn, M.; Heermann, D. W.; Lourenço, O.; Cordeiro, C. On the influence of topological catenation and bonding constraints on ring polymers. *Macromolecules* **2010**, *43*, 2564–2573.
- [25] Li, R.; Wen, X.; Huang, X.; Li, H.; Jiang, Z. Effects of ring sizes on the dynamic behaviors of [2] catenane. *Molecular Systems Design & Engineering* **2025**,
- [26] Li, J.; Zhang, B.; Li, Y. Glass formation in mechanically interlocked ring polymers: the role of induced chain stiffness. *Macromolecules* **2023**, *56*, 589–600.
- [27] Tubiana, L.; Ferrari, F.; Orlandini, E. Circular polycatenanes: Supramolecular structures with topologically tunable properties. *Physical Review Letters* **2022**, *129*, 227801.
- [28] Chiarantoni, P.; Micheletti, C. Effect of ring rigidity on the statics and dynamics of linear catenanes. *Macromolecules* **2022**, *55*, 4523–4532.
- [29] Rauscher, P. M.; Rowan, S. J.; de Pablo, J. J. Topological effects in isolated poly [n] catenanes: Molecular dynamics simulations and Rouse mode analysis. *ACS Macro Letters* **2018**, *7*, 938–943.
- [30] Dehaghani, Z. A.; Chubak, I.; Likos, C. N.; Ejtehadi, M. R. Effects of topological constraints on linked ring polymers in solvents of varying quality. *Soft Matter* **2020**, *16*, 3029–3038.
- [31] Pakula, T.; Jeszka, K. Simulation of single complex macromolecules. I. Structure and dynamics of catenanes. *Macromolecules* **1999**, *32*, 6821–6830.
- [32] Li, J.; Gu, F.; Yao, N.; Wang, H.; Liao, Q. Double asymptotic structures of topologically interlocked molecules. *ACS Macro Letters* **2021**, *10*, 1094–1098.
- [33] Rauscher, P. M.; Schweizer, K. S.; Rowan, S. J.; De Pablo, J. J. Thermodynamics and structure of poly [n] catenane melts. *Macromolecules* **2020**, *53*, 3390–3408.
- [34] Rauscher, P. M.; Schweizer, K. S.; Rowan, S. J.; de Pablo, J. J. Dynamics of poly [n] catenane melts. *The Journal of Chemical Physics* **2020**, *152*.
- [35] Hagita, K.; Murashima, T.; Sakata, N. Mathematical classification and rheological properties of ring catenane

- structures. *Macromolecules* **2021**, *55*, 166–177.
- [36] Chiarantoni, P.; Micheletti, C. Linear catenanes in channel confinement. *Macromolecules* **2023**, *56*, 2736–2746.
- [37] Caraglio, M.; Orlandini, E.; Whittington, S. Driven translocation of linked ring polymers through a pore. *Macromolecules* **2017**, *50*, 9437–9444.
- [38] Suma, A.; Micheletti, C. Pore translocation of knotted DNA rings. *Proceedings of the National Academy of Sciences* **2017**, *114*, E2991–E2997.
- [39] Li, K.; Wang, Y.; Guo, F.; He, L.; Zhang, L. Sliding dynamics of multi-rings on a semiflexible polymer in poly [n] catenanes. *Soft Matter* **2021**, *17*, 2557–2567.
- [40] Yasuda, Y.; Toda, M.; Mayumi, K.; Yokoyama, H.; Morita, H.; Ito, K. Sliding dynamics of ring on polymer in rotaxane: A coarse-grained molecular dynamics simulation study. *Macromolecules* **2019**, *52*, 3787–3793.
- [41] Mai, D. J.; Saadat, A.; Khomami, B.; Schroeder, C. M. Stretching dynamics of single comb polymers in extensional flow. *Macromolecules* **2018**, *51*, 1507–1517.
- [42] Lyulin, A. V.; Adolf, D. B.; Davies, G. R. Brownian dynamics simulations of linear polymers under shear flow. *The Journal of Chemical Physics* **1999**, *111*, 758–771.
- [43] Young, C. D.; Qian, J. R.; Marvin, M.; Sing, C. E. Ring polymer dynamics and tumbling-stretch transitions in planar mixed flows. *Physical Review E* **2019**, *99*, 062502.
- [44] Dutta, S.; Sing, C. E. Brownian dynamics simulations of bottlebrush polymers in dilute solution under simple shear and uniaxial extensional flows. *The Journal of Chemical Physics* **2024**, *160*.
- [45] Bayer, R.; Zachmann, H.; Calleja, F. B.; Umbach, H. Properties of elongational flow injection-molded polyethylene. Part 1: Influence of mold geometry. *Polymer Engineering & Science* **1989**, *29*, 186–192.
- [46] Sentmanat, M. L. Miniature universal testing platform: from extensional melt rheology to solid-state deformation behavior. *Rheologica Acta* **2004**, *43*, 657–669.
- [47] Starý, Z.; Papp, M.; Burghlea, T. Deformation regimes, failure and rupture of a low density polyethylene (LDPE) melt undergoing uniaxial extension. *Journal of Non-Newtonian Fluid Mechanics* **2015**, *219*, 35–49.
- [48] Martin, J. J.; Riederer, M. S.; Krebs, M. D.; Erb, R. M. Understanding and overcoming shear alignment of fibers during extrusion. *Soft Matter* **2015**, *11*, 400–405.
- [49] Weeks, J. D.; Chandler, D.; Andersen, H. C. Role of repulsive forces in determining the equilibrium structure of simple liquids. *The Journal of Chemical Physics* **1971**, *54*, 5237–5247.
- [50] Becerra, D.; Klotz, A. R.; Hall, L. M. Single-molecule analysis of solvent-responsive mechanically interlocked ring polymers and the effects of nanoconfinement from coarse-grained simulations. *The Journal of Chemical Physics* **2024**, *160*.
- [51] Ermak, D. L.; McCammon, J. A. Brownian dynamics with hydrodynamic interactions. *The Journal of Chemical Physics* **1978**, *69*, 1352–1360.
- [52] Ottinger, H. C. *Stochastic processes in polymeric fluids*; Springer, Berlin, 1996; Vol. 9.
- [53] Rotne, J.; Prager, S. Variational treatment of hydrodynamic interaction in polymers. *The Journal of Chemical Physics* **1969**, *50*, 4831–4837.
- [54] Yamakawa, H. Transport properties of polymer chains in dilute solution: hydrodynamic interaction. *The Journal of Chemical Physics* **1970**, *53*, 436–443.
- [55] Miao, L.; Young, C. D.; Sing, C. E. An iterative method for hydrodynamic interactions in Brownian dynamics simulations of polymer dynamics. *The Journal of Chemical Physics* **2017**, *147*.
- [56] Dünweg, B.; Reith, D.; Steinhauser, M.; Kremer, K. Corrections to scaling in the hydrodynamic properties of dilute polymer solutions. *The Journal of Chemical Physics* **2002**, *117*, 914–924.
- [57] Jendrejack, R. M.; Graham, M. D.; de Pablo, J. J. Hydrodynamic interactions in long chain polymers: Application of the Chebyshev polynomial approximation in stochastic simulations. *The Journal of Chemical Physics* **2000**, *113*, 2894–2900.
- [58] Jendrejack, R. M.; de Pablo, J. J.; Graham, M. D. Stochastic simulations of DNA in flow: Dynamics and the effects of hydrodynamic interactions. *The Journal of Chemical Physics* **2002**, *116*, 7752–7759.
- [59] Knoll, D. A.; Keyes, D. E. Jacobian-free Newton–Krylov methods: a survey of approaches and applications. *Journal of Computational Physics* **2004**, *193*, 357–397.
- [60] Pernice, M.; Walker, H. F. NITSOL: A Newton iterative solver for nonlinear systems. *SIAM Journal on Scientific Computing* **1998**, *19*, 302–318.
- [61] Zhou, Y.; Hsiao, K.-W.; Regan, K. E.; Kong, D.; McKenna, G. B.; Robertson-Anderson, R. M.; Schroeder, C. M. Effect of molecular architecture on ring polymer dynamics in semidilute linear polymer solutions. *Nature Communications* **2019**, *10*, 1753.
- [62] Bird, R. B.; Armstrong, R. C.; Hassager, O. *Dynamics of Polymeric Fluids*, Fluid Mechanics. 1977.
- [63] Graham, M. D. *Microhydrodynamics, Brownian Motion, and Complex Fluids*; Cambridge Texts in Applied Mathematics; Cambridge University Press, 2018; p 170–200.
- [64] Bosko, J. T.; Ravi Prakash, J. Effect of molecular topology on the transport properties of dendrimers in dilute solution at Θ temperature: A Brownian dynamics study. *The Journal of Chemical Physics* **2008**, *128*.
- [65] Schroeder, C. M.; Teixeira, R. E.; Shaqfeh, E. S.; Chu, S. Dynamics of DNA in the flow-gradient plane of steady shear flow: Observations and simulations. *Macromolecules* **2005**, *38*, 1967–1978.
- [66] Saha Dalal, I.; Albaugh, A.; Hoda, N.; Larson, R. G. Tumbling and deformation of isolated polymer chains in shearing flow. *Macromolecules* **2012**, *45*, 9493–9499.
- [67] De Gennes, P. Coil-stretch transition of dilute flexible polymers under ultrahigh velocity gradients. *The Journal of Chemical Physics* **1974**, *60*, 5030–5042.
- [68] Smith, D. E.; Babcock, H. P.; Chu, S. Single-polymer dynamics in steady shear flow. *Science* **1999**, *283*, 1724–1727.
- [69] Teixeira, R. E.; Babcock, H. P.; Shaqfeh, E. S.; Chu, S. Shear thinning and tumbling dynamics of single polymers in the flow-gradient plane. *Macromolecules* **2005**, *38*, 581–592.
- [70] Krigbaum, W.; Flory, P. Molecular weight dependence of the intrinsic viscosity of polymer solutions. II. *Journal of Polymer Science* **1953**, *11*, 37–51.
- [71] Brereton, M. The statistical mechanics of a concatenated polymer chain. *Journal of Physics A: Mathematical and General* **2001**, *34*, 5131.
- [72] Noda, Y.; Hayashi, Y.; Ito, K. From topological gels to slide-ring materials. *Journal of Applied Polymer Science* **2014**, *131*.

- [73] Raphaël, E.; Gay, C.; De Gennes, P. Progressive construction of an “Olympic” gel. *Journal of Statistical Physics* **1997**, *89*, 111–118.
- [74] Speed, S.; Atabay, A.; Peng, Y.-H.; Gupta, K.; Müller, T.; Fischer, C.; Sommer, J.-U.; Lang, M.; Krieg, E. Assembling a true ‘Olympic Gel’ from over 16,000 combinatorial DNA rings. *bioRxiv* **2024**, 2024–07.
- [75] Chen, D.; Panyukov, S.; Sapir, L.; Rubinstein, M. Elasticity of Slide-Ring Gels. *ACS Macro Letters* **2023**, *12*, 362–368.
- [76] Tanahashi, K.; Koga, T. Molecular Simulation and Theoretical Analysis of Slide-Ring Gels under Biaxial Deformation. *Gels* **2021**, *7*, 129.
- [77] Uehara, S.; Wang, Y.; Ootani, Y.; Ozawa, N.; Kubo, M. Molecular-level elucidation of a fracture process in slide-ring gels via coarse-grained molecular dynamics simulations. *Macromolecules* **2022**, *55*, 1946–1956.
- [78] Yasuda, Y.; Masumoto, T.; Mayumi, K.; Toda, M.; Yokoyama, H.; Morita, H.; Ito, K. Molecular dynamics simulation and theoretical model of elasticity in slide-ring gels. *ACS Macro Letters* **2020**, *9*, 1280–1285.
- [79] Müller, T.; Sommer, J.-U.; Lang, M. Tendoners–force sensitive bis-rotaxanes with jump-like deformation behavior. *Soft Matter* **2019**, *15*, 3671–3679.
- [80] Müller, T.; Sommer, J.-U.; Lang, M. Swelling of tendoners gels. *Macromolecules* **2021**, *54*, 4601–4614.
- [81] Müller, T.; Sommer, J.-U.; Lang, M. Elasticity of tendoners gels. *Macromolecules* **2022**, *55*, 7540–7555.
- [82] Frisch, H.; Martin, I.; Mark, H. Zur Struktur der Polysiloxene. I. *Monatshefte für Chemie und verwandte Teile anderer Wissenschaften* **1953**, *84*, 250–256.
- [83] Patat, F.; Derst, P. Über den thermischen Abbau des polymeren Phosphornitridchlorids. *Angewandte Chemie* **1959**, *71*, 105–110.
- [84] Larson, R. Analysis of polymer turbulent drag reduction in flow past a flat plate. *Journal of Non-Newtonian Fluid Mechanics* **2003**, *111*, 229–250.
- [85] Perkins, T. T.; Smith, D. E.; Chu, S. Single polymer dynamics in an elongational flow. *Science* **1997**, *276*, 2016–2021.
- [86] Dimitropoulos, C. D.; Sureshkumar, R.; Beris, A. N. Direct numerical simulation of viscoelastic turbulent channel flow exhibiting drag reduction: effect of the variation of rheological parameters. *Journal of Non-Newtonian Fluid Mechanics* **1998**, *79*, 433–468.
- [87] Paterson, R. W.; Abernathy, F. Turbulent flow drag reduction and degradation with dilute polymer solutions. *Journal of Fluid Mechanics* **1970**, *43*, 689–710.
- [88] Chao, K.; Child, C.; Grens, E.; Williams, M. Antimisting action of polymeric additives in jet fuels. *AIChE Journal* **1984**, *30*, 111–120.
- [89] Wei, M.-H.; Li, B.; David, R. A.; Jones, S. C.; Sarohia, V.; Schmitigal, J. A.; Kornfield, J. A. Mega-supramolecules for safer, cleaner fuel by end association of long telechelic polymers. *Science* **2015**, *350*, 72–75.
- [90] Lhota, R. C.; Learsch, R. W.; Temme, J.; Coburn, V.; Kornfield, J. A. Mist-control of polyalphaolefin (PAO) lubricants using long pairwise end-associative polymers. *Journal of Non-Newtonian Fluid Mechanics* **2024**, *326*, 105197.
- [91] Zhang, M.; De Bo, G. Mechanical susceptibility of a rotaxane. *Journal of the American Chemical Society* **2019**, *141*, 15879–15883.
- [92] Lee, B.; Niu, Z.; Craig, S. L. The mechanical strength of a mechanical bond: sonochemical polymer mechanochemistry of poly (catenane) copolymers. *Angewandte Chemie International Edition* **2016**, *55*, 13086–13089.

APPENDIX

Appendix A: Equilibrium Properties

TABLE A.1: Equilibrium properties of linear polymers

M_w	R_g^2/a^2	$D_{COM}\zeta/k_B T$	τ_R/τ
40	78.17	0.1649	79.02
72	148.09	0.1196	206.35
80	186.30	0.1119	277.41
120	276.76	0.0892	517.26

TABLE A.2: Equilibrium properties of polyrotaxanes

M_w	N_{bb}	N_{rings}	R_g^2/a^2	$D_{COM}\zeta/k_B T$	τ_R/τ
56	40	2	119.98	0.1433	139.57
72	40	4	125.82	0.1373	152.78
88	40	6	133.52	0.1312	169.60
104	40	8	143.14	0.1256	189.94
112	80	4	237.04	0.0992	398.37
144	80	8	263.23	0.0932	470.75
176	80	12	303.02	0.0871	579.55
208	80	16	341.24	0.0823	690.90
168	120	6	349.41	0.0801	727.28
216	120	12	455.36	0.0730	1040.23
264	120	18	507.79	0.0686	1234.32
312	120	24	567.62	0.0643	1470.45

TABLE A.3: Equilibrium properties of daisy chains

M_w	BPS	N_{seg}	R_g^2/a^2	$D_{COM}\zeta/k_B T$	τ_R/τ
30	8	2	20.49	0.2504	13.64
74	8	4	61.01	0.1624	62.61
118	8	6	116.86	0.1254	155.26
206	8	10	247.67	0.0914	451.62
46	16	2	46.10	0.1874	41.01
106	16	4	125.10	0.1228	169.84
166	16	6	202.98	0.0972	347.90
226	16	8	307.33	0.0811	631.57
78	32	2	103.86	0.1331	130.08
170	32	4	279.14	0.0872	533.57
262	32	6	472.17	0.0687	1145.30

TABLE A.4: Equilibrium properties of polycatenanes

M_w	BPR	N_{rings}	R_g^2/a^2	$D_{COM}\zeta/k_B T$	τ_R/τ
16	8	2	7.12	0.3544	3.35
40	8	5	21.49	0.2396	14.91
80	8	10	54.14	0.1685	53.74
168	8	21	145.80	0.1122	217.18
344	8	43	373.70	0.0745	835.88
520	8	65	621.31	0.0590	1753.85
160	16	10	117.34	0.1133	172.67
240	24	10	184.25	0.0898	341.97
320	32	10	275.50	0.0751	611.21

Appendix B: Additional Shear Flow Properties

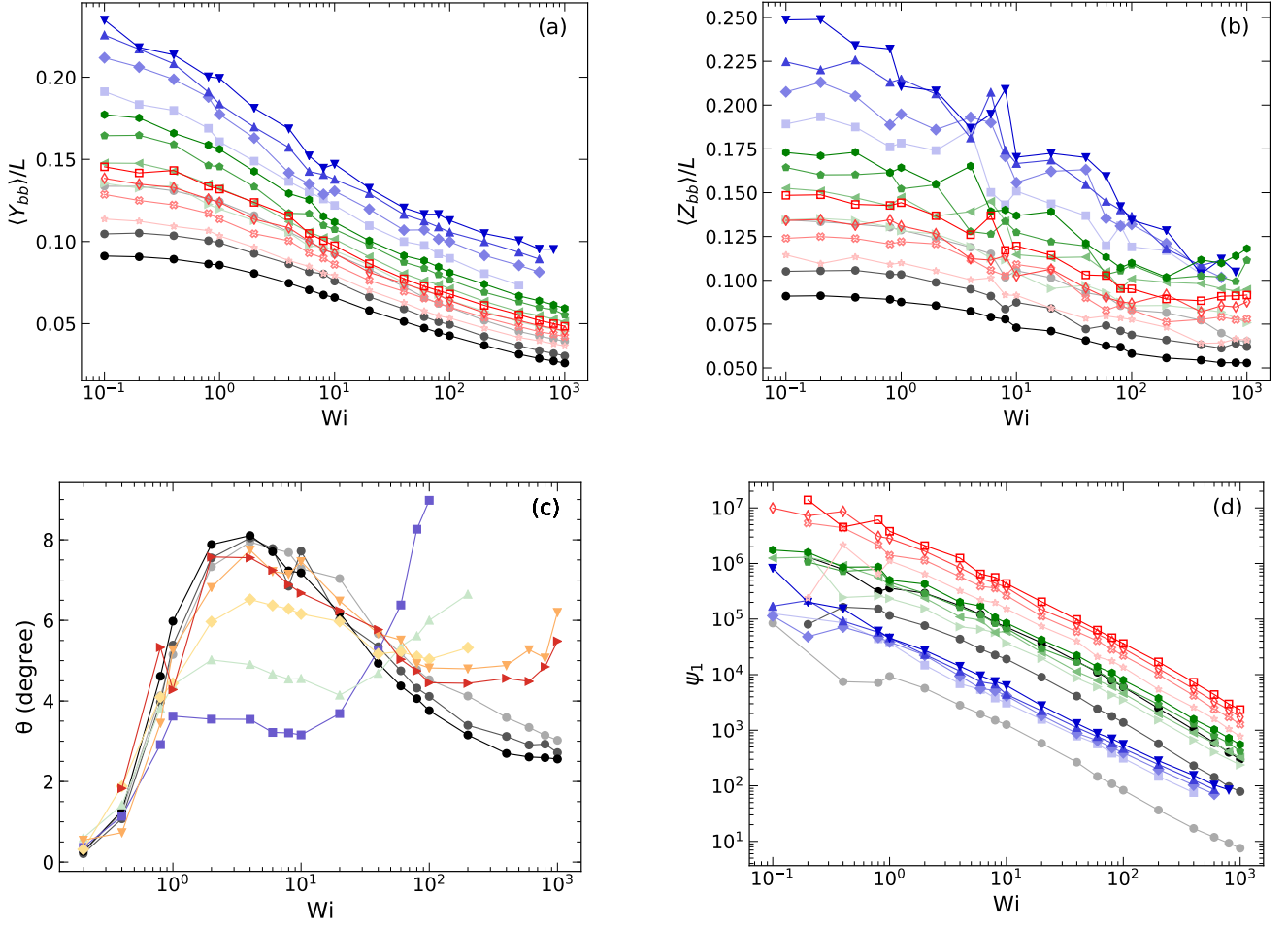


FIG. B.1: Polyrotaxane properties in shear flow as a function of Weissenberg number (Wi): (a) fractional extension in gradient direction ($\langle Y_{bb} \rangle / L$), (b) fractional extension in cross direction ($\langle Z_{bb} \rangle / L$), (c) orientation angle (θ), and (d) first normal stress coefficient (Ψ_1). Linear polymers are shown in shades of gray with darker shades indicating more beads. Polyrotaxanes with 40, 80, and 120 backbone beads (N_{bb}) are shown in blue, green, and red, respectively; darker shades indicate higher ring density (N_{rings}/N_{bb}). The rings in the polyrotaxanes are composed of 8 beads, regardless of backbone length.

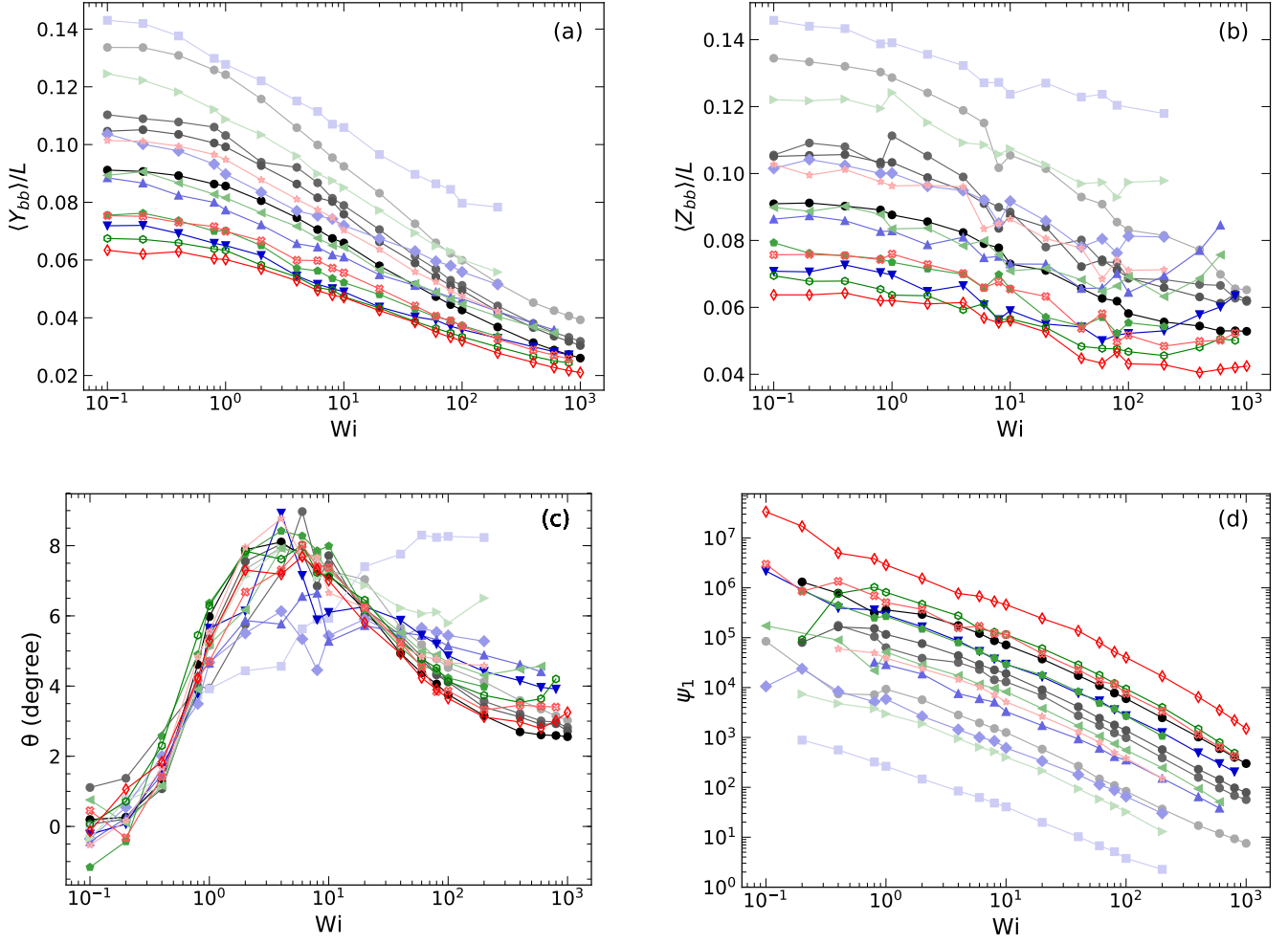


FIG. B.2: Daisy chain properties in shear flow as a function of Weissenberg number (Wi): (a) fractional extension in gradient direction ($\langle Y_{bb} \rangle / L$), (b) fractional extension in cross direction ($\langle Z_{bb} \rangle / L$), (c) orientation angle (θ), and (d) first normal stress coefficient (Ψ_1). Linear polymers are shown in shades of gray with darker shades indicating more beads. Daisy chains with 8, 16, and 32 beads per segment (BPS) are shown in blue, green, and red, respectively; darker shades indicate more segments (N_{seg}). The rings in all daisy chains are composed of 8 beads.

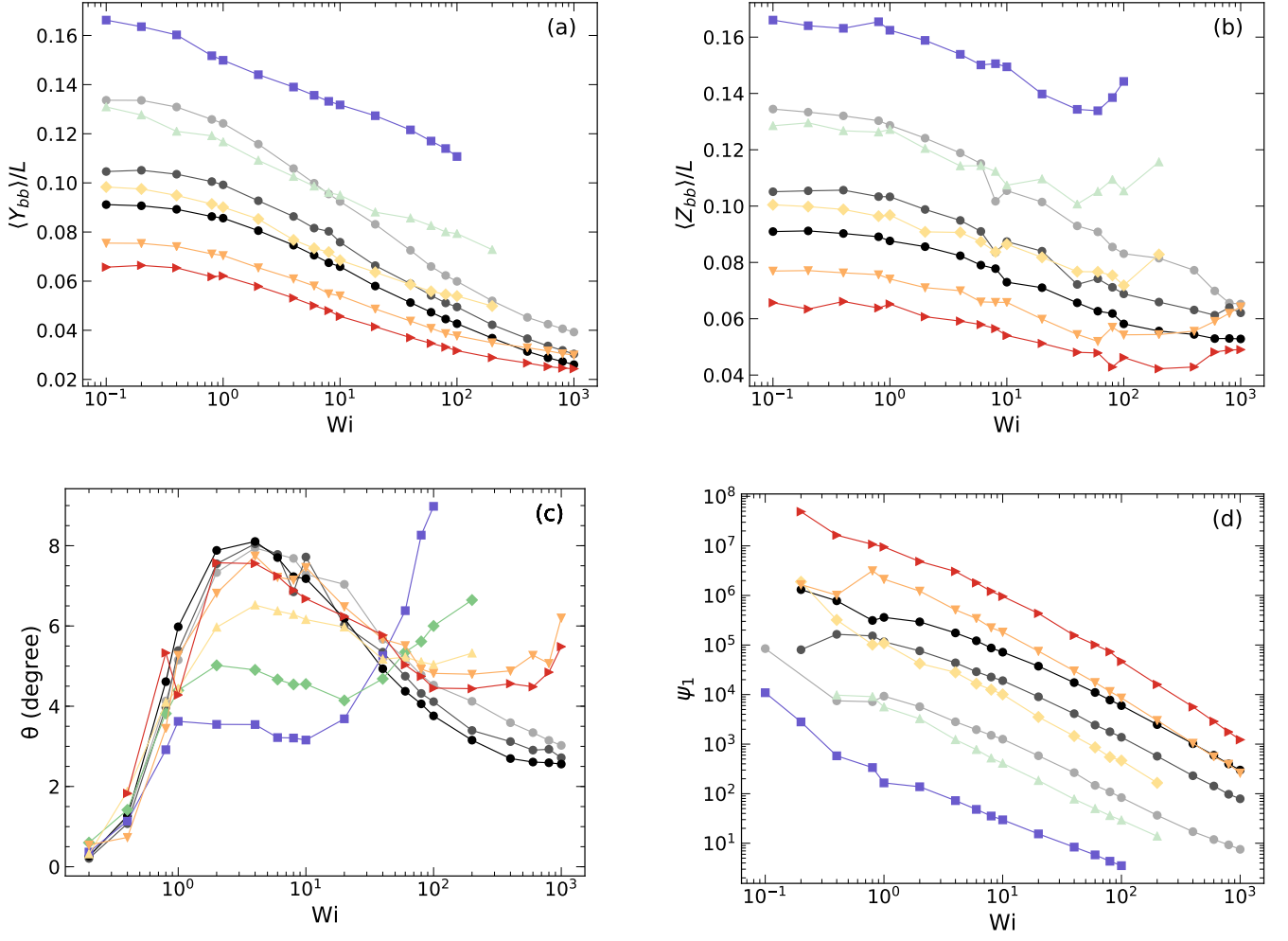


FIG. B.3: Polycatenane properties in shear flow as a function of Weissenberg number (Wi): (a) fractional extension in gradient direction ($\langle Y_{bb} \rangle / L$), (b) fractional extension in cross direction ($\langle Z_{bb} \rangle / L$), (c) orientation angle (θ), and (d) first normal stress coefficient (ψ_1). Linear polymers are shown in shades of gray with darker shades indicating more beads. Colors from cold to hot indicate higher number of rings (N_{rings}) with fixed beads per ring ($BPR = 8$).

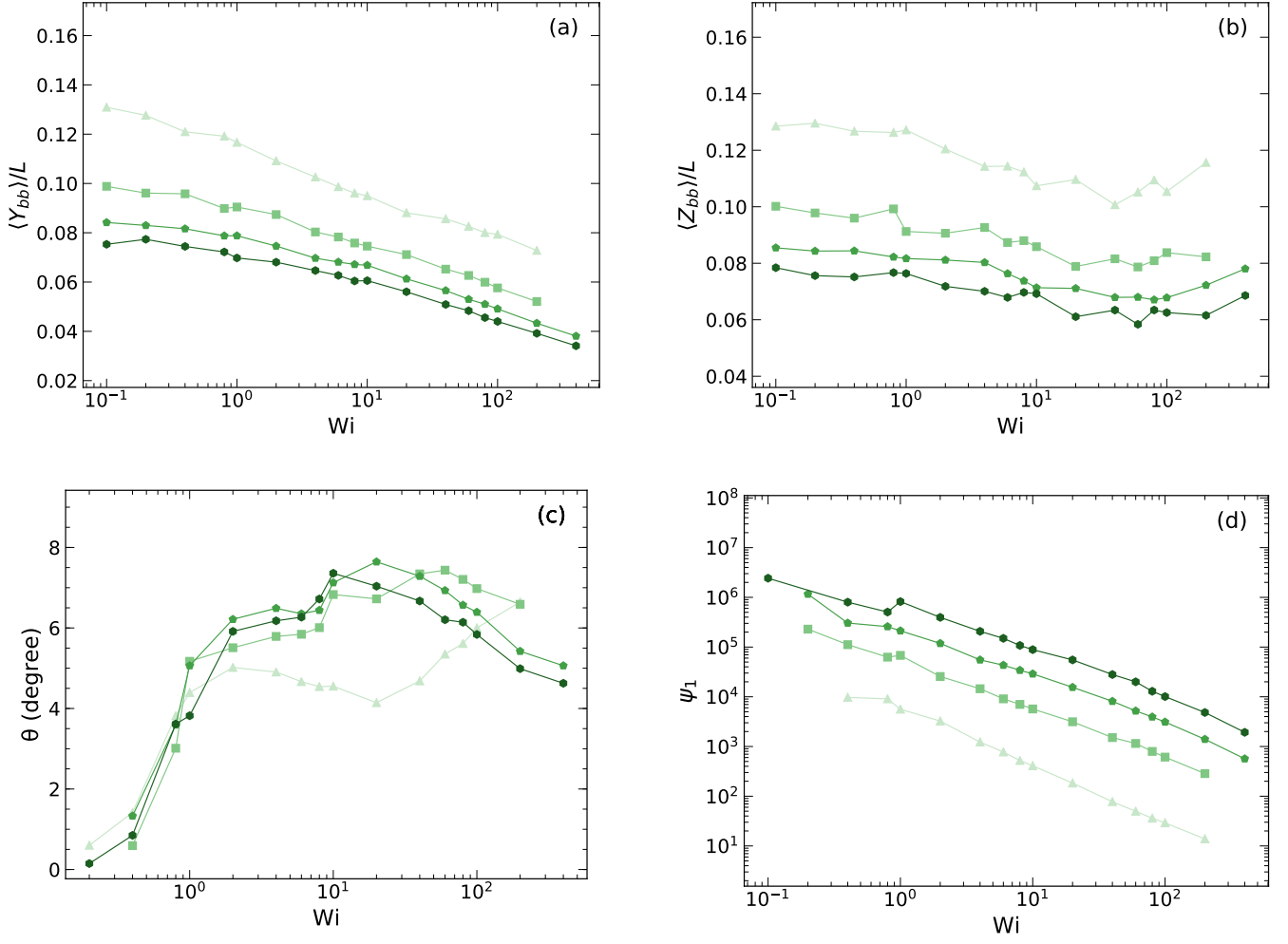


FIG. B.4: Polycatenane properties in shear flow as a function of Weissenberg number (Wi): (a) fractional extension in gradient direction ($\langle Y_{bb} \rangle / L$), (b) fractional extension in cross direction ($\langle Z_{bb} \rangle / L$), (c) orientation angle (θ), and (d) first normal stress coefficient (Ψ_1). Darker shades indicate higher beads per ring (BPR) in polycatenanes with fixed number of rings ($N_{\text{rings}} = 10$).

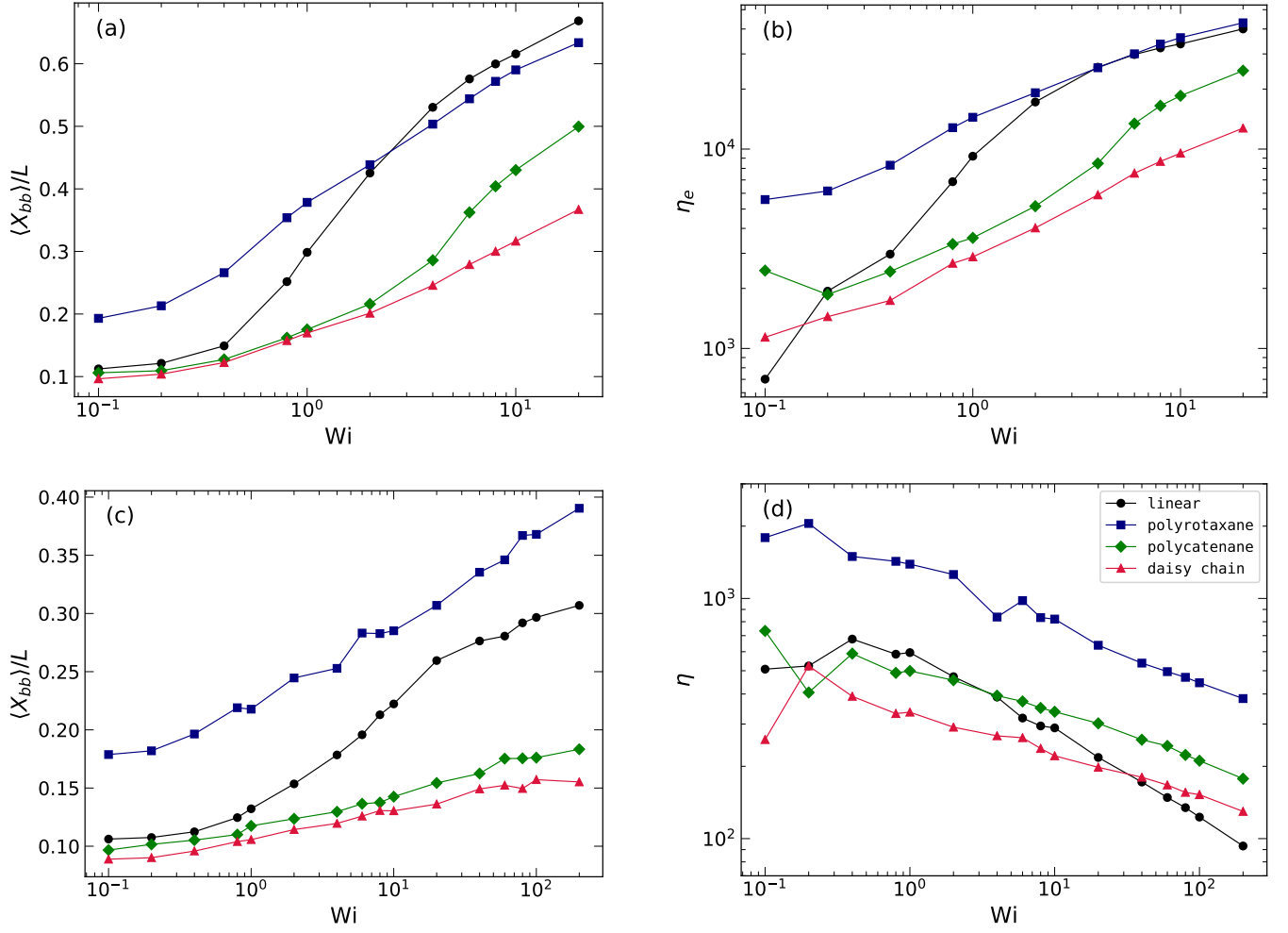


FIG. B.5: Comparison of linear and MIP polymers of similar maximum contour length (L) in extensional (a, b) and shear (c, d) flow. Fractional extension in the flow direction ($\langle X_{bb} \rangle / L$) for extension (a) and shear (c) along with extensional viscosity (η_e) (b) and shear viscosity (η) are given as a function of Weissenberg number (Wi). The linear polymer (black) has 80 backbone beads. The polyrotaxane (blue) has 80 backbone beads including 2 capping beads and 16 rings. The daisy chain (green) has 6 linear segments of 8 beads each interlocked with 10 8 bead rings and includes 2 capping beads. The polycatenane (red) has 10 interconnected rings of 16 beads each.